A marked point process of rectangles and segments for automatic analysis of Digital Elevation Models

Mathias Ortner, Xavier Descombes, Josiane Zerubia

▶ **To cite this version:**

Mathias Ortner, Xavier Descombes, Josiane Zerubia. A marked point process of rectangles and segments for automatic analysis of Digital Elevation Models. [Research Report] RR-5712, INRIA. 2006, pp.42. inria-00070305

HAL Id: inria-00070305
https://inria.hal.science/inria-00070305

Submitted on 19 May 2006

HAL is a multi-disciplinary open access archive for the deposit and dissemination of scientific research documents, whether they are published or not. The documents may come from teaching and research institutions in France or abroad, or from public or private research centers.

L'archive ouverte pluridisciplinaire **HAL**, est destinée au dépôt et à la diffusion de documents scientifiques de niveau recherche, publiés ou non, émanant des établissements d'enseignement et de recherche français ou étrangers, des laboratoires publics ou privés.

INRIA

INSTITUT NATIONAL DE RECHERCHE EN INFORMATIQUE ET EN AUTOMATIQUE

A marked point process of rectangles and segments for automatic analysis of Digital Elevation Models.

Mathias Ortner — Xavier Descombes — Josiane Zerubia

N° 5712

Octobre 2005

Thème COG

ISSN 0249-6399 ISRN INRIA/RR--5712--FR+ENG

INRIA
SOPHIA ANTIPOLIS

A marked point process of rectangles and segments for automatic analysis of Digital Elevation Models.

Mathias Ortner, Xavier Descombes, Josiane Zerubia*

Thème COG — Systèmes cognitifs
Projet Ariana

Rapport de recherche n° 5712 — Octobre 2005 — 42 pages

Abstract: This work presents a framework for automatic feature extraction from images using stochastic geometry. Features in images are modeled as realizations of a spatial point process of geometrical shapes. This framework allows the incorporation of a prior knowledge on the spatial repartition of features. More specifically, we present a model based on the superposition of a process of segments and a process of rectangles. The former is dedicated to the detection of linear networks of discontinuities, while the latter aims at segmenting homogeneous areas. An energy is defined, favoring connections of segments, alignments of rectangles, as well as a relevant interaction between both types of objects. The estimation is performed by minimizing the energy using a simulated annealing algorithm.

The proposed model is applied to the analysis of Digital Elevation Models (DEMs). These images are raster data representing the altimetry of a dense urban area. We present results on real data provided by the IGN (French National Geographic Institute) consisting in low quality DEMs of various types.

Key-words: Image processing, spatial point process, stochastic geometry, dense urban area, Digital Elevation Models, Laser data, land register, building detection, MCMC, RJMCMC, simulated annealing.

* Ariana - Joint research group CNRS / INRIA / UNSA - INRIA, 2004 route des Lucioles, BP 93, Sophia Antipolis, France. Tel : +33 492 387 857, Fax : +33 492 387 643, Email : ortner@ece.uic.edu, xavier.descombes@sophia.inria.fr, josiane.zerubia@sophia.inria.fr

Un processus ponctuel marqué de segments et de rectangles pour l'analyse automatique de modèles numériques d'élévation.

Résumé : Ce travail présente une approche par géométrie stochastique pour l'extraction de primitives dans les images. Ces structures sont modélisées sous forme de réalisations d'un processus ponctuel spatial marqué dont les points sont des formes géométriques. Cette approche permet d'incorporer un modèle *a priori* sur la répartition spatiale des structures d'intérêt. Plus spécifiquement, nous présentons un modèle fondé sur l'interaction d'un processus de rectangles avec un processus de segments. Le premier est dédié à la détection des zones homogènes dans l'image et le second à la détection des discontinuités significatives. Nous définissons l'énergie d'une configuration de façon à favoriser la connection entre les segments, l'alignement des rectangles et l'adéquation entre les deux types de primitives. L'estimation repose sur l'emploi d'une technique de recuit-simulé.

Le modèle proposé est appliqué à l'analyse de Modèles Numériques d'Elevation. Nous présentons des résultats sur des données réelles fournies par l'Institut Géographique National (IGN). Nous montrons en particulier que l'approche est efficace sur des données de types très différents.

Mots-clés : Traitement des images, processus ponctuels spatiaux, géiométrie stochastique, zones urbaines denses, données Laser, détection de bâtiments, MCMC, RJMCMC, recuit-simulé.

Contents

1 Introduction

1.1 Dense urban areas and building reconstruction

As cities are the place of increasing concentrations of people they are the centers of numerous interests: economical, military, environmental, to name but a few. 3D cities representations are of first interest for different communities (telecommunications, security, etc...). However, automatically obtaining such representations is still an open issue.

The remote sensing community provides various sensors and techniques to accumulate data on a specific urban area. In particular, the advent of high resolution data (HR) in remote sensing has given aerial and satellite images a primary role in analyzing urban areas. Other imaging techniques like LASER or LIDAR sensors provide different data. However, the complexity of urban areas make the data challenging for automatic analysis.

In this work, we focus on the analysis of Digital Elevation Models (DEMs). DEMs are raster data representing the altimetry of an urban area. They consist in 2D images such that the gray level of a pixel describes the height of the corresponding point in the scene. This type of data is obtained through different sensors and processing techniques (e.g. stereovision, laser sensing, etc...). The sample presented in Figure 1 is a typical example of a Digital Elevation Model obtained by aerial stereovision.

Extraction of buildings from urban data has been subject to a corpus of literature. General overviews can be found in [3, 12] or in the introduction of [9]. Automatic methods are mostly made up of three steps. The *focalization step* selects a relevant area that supposedly corresponds to a building. A pre-segmentation (ground/above ground) or the incorporation of external vectorial data (e.g. a land register) are usual ways of achieving this pre-selection. The two next steps, namely the *primitive detection* and the *building reconstruction* are usually closely linked. The *bottom up* process creates aggregations of primitives (illustrated for instance, in [3]), while the *top-down* procedure matches the obtained aggregation hypothesis with building models. The association of hypothetical aggregations with pre-defined building models is a combinatorial problem and thereby concentrates most of the computational load of the procedure.

As the structure of dense urban areas is tremendously complex, there is a huge need for incorporating as much information as possible. The fusion of different types of data is a first possibility. Many proposed methods tend to increase the variety of data used by including multiple color images, Laser clouds of points, register maps or hyperspectral images (see examples in [9, 4, 5]). Additional information can also be integrated under the form of a *prior knowledge*. Proposing a set of possible building shapes is a first way of incorporating a prior knowledge. Our approach allows going further. We propose to incorporate a knowledge on the patterns of the primitives to be extracted in terms of interactions between objects.

1.2 Our approach: spatial point process models

Our approach consists in modeling an urban area by a set of an *unknown number* of interacting particles, where each particle stands for a building element. A particle is eventually a geometrical object that can be compared to the data.

In [17] we present an original approach and model cities as realizations of a spatial point process of rectangles. For each rectangle a data energy is defined, correlating possible rectangle hypothesis with the data. A regularizing energy acting on the spatial pattern of rectangles is incorporated. For instance, alignments between buildings are favored. This model is robust with respect to the type and the quality of the data, but fails to process very noisy data.

In this report, we extend our previous work by examining the possibility of dealing with such noisy data. Our previous work showed robustness, due to the type of prior used acting on the spatial patterns of extracted features. We show in this paper that the point process approach allows the fusion

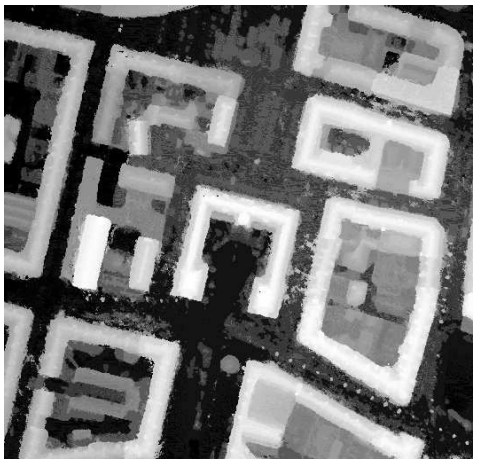

Figure 1: Digital Elevation Model of Amiens (©IGN). The darker a pixel, the lower the height of the corresponding point in the scene.

of different informations. We focus on the example of homogeneous regions and linear discontinuities, and propose a model of interacting point processes of rectangles and segments.

1.3 History of point processes in image processing

Point process models in image processing can be seen as a natural extension of Markov Random Field approaches (MRFs). In the early eighties, MRFs have been introduced in the computer vision community through the works of Besag [2] and Geman and Geman [6]. In a Markov Random Field representation, an image is modeled as a realization of a collection of random values associated with each pixel in the image. Although these pixel-based approaches proved to be powerful for the analysis of dense urban areas at medium resolutions (e.g. classification of textures [27]), the advent of HR data has strengthened the need for approaches amenable to the consideration of the geometrical nature of urban scenes.

Point processes models - that can be considered as a part of the wider "stochastic geometry" field, allow the modeling of images as random configurations of geometric shapes and provide a natural setup for the inclusion of a prior knowledge on the spatial pattern of features. Such models were first used in image processing by A. Baddeley and M.N.M. van Lieshout in [1]. Further work has been performed by H. Rue ([19,20]) and Green [18] while more complex applications, like road or building extraction, have been studied in [23, 11, 17, 13, 10]. Different ideas have been explored by Grenander, Miller and Sivrastava under the name of "pattern theory" (see [21] and reference therein), although the objects were not interacting.

1.4 Outline of the report

In Section 2 we provide a general discussion on point process models for automatic image feature extraction. We propose a generic model amenable to the inclusion of a prior knowledge on the pattern of features. In Section 3, we then present the specific segment and rectangle point process models we adopted. Segments are used for detecting discontinuities, while rectangles are used for segmenting homogeneous areas. In Section 4, we provide an overview of the employed Reversible Jump Monte Carlo Markov Chain (RJMCMC) algorithm. We finally present and discuss results obtained on real data in Section 5.

2 Point process models for image feature extraction

2.1 Introduction to point processes

2.1.1 Support, images and DEMs

We model images as a *continuous* bounded set $K = [0, X_{1_{max}}] \times [0, X_{2_{max}}]$, and note $x = (c_1, c_2)$ a point of K. A Digital Elevation Model can therefore be modelled as a function associating a height with points of K. In the following, we note by H such a function: $H : K \to [0, \infty[$.

2.1.2 Random configuration of points

A *configuration of points* $\mathbf{x}$ (noted in bold) is a unordered set of points in K

$$\mathbf{x} = \{x_1, \ldots, \mathbf{x}_{n(\mathbf{x})}\}, \qquad x_i \in K, \tag{1}$$

where $n(\mathbf{x}) = \text{card}(\mathbf{x})$ denotes the number of points in the configuration. We note $\mathcal{C}$ the set of all possible finite configurations.

Let consider a mapping from an abstract probability space $(\Omega, \mathcal{A}, \mathbf{P})$ to the set of configurations $\mathcal{C}$. Due to the finiteness of the considered configurations along with the boundedness of K, the σ-algebra associated with $\mathcal{C}$ is well defined (see [26] for details.)

A *point process* $\mathbf{X}$ of points in K is a measurable mapping

$$\forall \omega \in \Omega, \quad \mathbf{X}(\omega) = \{x_1, \ldots, x_n, \ldots\} \;\; x_i \in K. \tag{2}$$

Accordingly, a point process is a random variable whose realizations are random configurations of points.

2.1.3 Poisson point process

The most random point process (in the entropy sense) is the *Poisson point process*. Let $\nu(.)$ be a positive measure on K. A Poisson point process $\mathbf{X}$ with intensity $\nu(.)$ verifies the following properties

- for every Borel set $A \subset K$, the random variable $N_{\mathbf{X}}(A)$, giving for the number of points of $\mathbf{X}$ falling in the set A, follows a discrete Poisson distribution with mean $\nu(A)$

$$\mathbf{P}(N_{\mathbf{X}}(A) = n) = e^{-\nu(A)} \frac{\nu(A)^n}{n!}, \tag{3}$$

- and for every finite sequence of non intersecting Borelian sets $B_1, \ldots, B_p$ the corresponding random variables $N_{\mathbf{X}}(B_1), \ldots, N_{\mathbf{X}}(B_p)$ are independent.

Poisson point processes are usefull in our setup due to their analog role to Lebesgue measures on $\mathbb{R}^d$. As we detail it later, it is indeed possible to define point processes by their density with respect to the distribution of a reference Poisson point process.

2.1.4 Marked point process

The configurations of points described so far only include simple points of $\mathbb{R}^2$. To describe random configurations of geometrical objects, random marks are added to each point.

For instance, let consider the following mark set

$$M^r = [-\frac{\pi}{2}, \frac{\pi}{2}] \times [L^r_{\min}, L^r_{\max}] \times [l^r_{\min}, l^r_{\max}]. \tag{4}$$

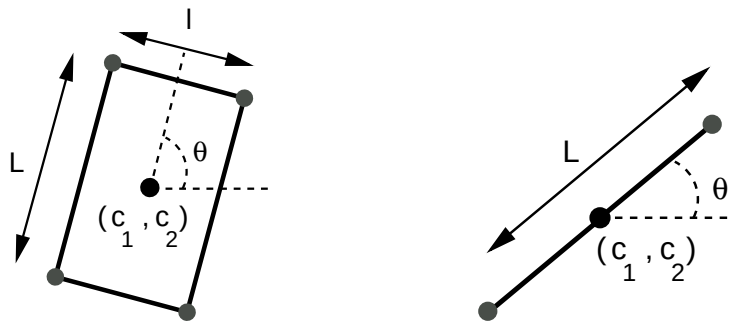

Figure 2: Adopted parameterizations of segments and rectangles

Noting by x elements of $S_r = K \times M_r$, we consider the following parameterization describing rectangles

$$x \in S_r, \quad x = (c_1(x), c_2(x), \theta(x), L(x), l(x)) \,, \tag{5}$$

where $(c_1(x), c_2(x))$, $\theta(x)$, $L(x)$ and $l(x)$ correspond respectively to the center position, the orientation, the length and the width of the rectangle x. A marked point process $\mathbf{X}$ of rectangles is a point process on $S_r = K \times M_r$ [1]. This parameterization is illustrated on Figure 2.

Similarly, we define a mark set M_s to describe segments

$$M_s = [-\frac{\pi}{2}, \frac{\pi}{2}] \times [L^s_{min}, L^s_{max}]. \tag{6}$$

We note y an element of $S_s = K \times M_s$ representing a segment

$$y \in S_s, \quad y = (c_1(y), c_2(y), \theta(y), L(y)), \tag{7}$$

and use $\mathbf{Y}$ to denote a point process of segments.

Finally, we note $\mathcal{C}_r$ and $\mathcal{C}_s$ the sets of finite configurations of rectangles and segments.

2.1.5 Density of a spatial point process

An attractive feature of spatial point processes is the possibility of defining a point process distribution by its *probability density function* (pdf). A Poisson point process can indeed play the analog role to Lebesgue measure on $\mathbb{R}^d$.

Consider the distribution $\mu(.)$ of a Poisson point process defined by its non atomic intensity measure $\nu(.)$ and a mapping $h(.)$ from the space of configurations of points $\mathcal{C}$ to $[0, \infty[$. We consider the function $Z(\mu, h)$ defined as

$$Z = \int_{\mathcal{C}} h(\mathbf{x}) d\mu(\mathbf{x}). \tag{8}$$

If $Z < \infty$, the function $Z^{-1}h(\mathbf{x})$ can be seen as the density of a point process $\mathbf{X}$ with respect to the reference Poisson process (see [26]).

For instance, assume that

$$h(\mathbf{x}) = \prod_{i=1}^{n(\mathbf{x})} \beta(x_i) \tag{9}$$

where $\beta(.)$ is an *intensity* function from S to $]0, \infty[$. A point process $\mathbf{X}$ defined by this density turns to be a Poisson point process with intensity

$$\nu'(A) = \int_A \beta(u) d\nu(u). \tag{10}$$

[1] There is actually a further requirement that the restriction of $\mathbf{X}$ to K, noted $\mathbf{X}_{|K}$, should also be a point process on K. In our case, this technical condition on the measurability of the mapping $\mathbf{X}$ is satisfied since the sets K and S_r are bounded, see [26] for details.

In this simple case, the probability density function $Z^{-1}h(.)$ allows a change of intensity measure. This example actually belongs to the more general class of *exponential families*. Let $t(.)$ be a mapping from $\mathcal{C}$ to $\mathbb{R}^k$. It is possible to describe a class of point process densities by using a parameter $\theta \in \mathbb{R}^k$ together with the scalar product $< ., . >$

$$h(\mathbf{x}) = e^{-<\theta, t(\mathbf{x})>} \tag{11}$$

Of course, the density is well defined if and only if $Z(\theta, \mu) < \infty$. In this work we introduce a density where points are not independent but are correlated by means of interaction energies.

2.1.6 Estimator and MCMC

In [16] we presented an MCMC algorithm generating samples of a point process $\mathbf{X}$ defined by an unnormalized density $h(.)$ along with a reference Poisson point process distribution. The obtained algorithm produces a Markov Chain $(X_t)_{t\geq 0}$ ergodically converging to the distribution of $\mathbf{X}$.

The procedure permits the computation of Monte Carlo values. Another possibility is to use the sampler within a *simulated annealing* framework providing a global maximum of the density $h(.)$ as described in [25]. The estimator obtained is consequently the maximum density estimator

$$\hat{\mathbf{x}} = \text{Argmax } h(.) \tag{12}$$

The algorithm is detailed in Section 4.

2.2 Point process models for image feature extraction

In this section, we define a suitable class of densities for the extraction of features in Digital Elevation Models. As mentioned previously, we focus on two types of elements: segments and rectangles. Our goal is to use the segments for detecting discontinuities and the rectangles to detect rectangular homogeneous areas standing for buildings. We therefore need to define a density making the objects fit the data (homogeneity for rectangles, discontinuity for segments) as well as favoring some patterns (connections of segments, interactions between segments and rectangles). In this section, we focus on generic modeling issues while the specific models are detailed in section 3.

Configurations of objects, image and energy. Let consider a point process $\mathbf{X}$ of features (e.g. either segments or rectangles). We recall here the strategy we adopted in [17] to define a suitable unnormalized density $h(.)$. In image processing, two main types of models are generally used. The first approach, *Bayesian modeling*, is known to be powerful but requires to exhibit a likelihood function describing the distribution of an image I for a fixed configuration $\mathbf{x}$ of features (conditional distribution). The second approach uses the Gibbs distribution associated with a suitable energy function.

In our framework, the Bayesian approach would necessitate to accurately describe the distribution of heights in every pixel of the DEM for a fixed configuration of elements. This is a hard task, since by definition a feature only contains a small part of the image information. Examples of Bayesian point process models are given in [18] or [19]. They rely on the use of foreground and background models of grey level distribution. In [15] we proposed a Bayesian model for building extraction based on a point process of 3D buildings. The computational price for having a complete conditional description of the image is too heavy as it requires too many random parameters.

In this work, we use the second class of widely used models and define a density under its Gibbs form

$$h(.) = \frac{1}{Z} e^{-U(\mathbf{x})} \quad U(\mathbf{x}) = U_{int}(\mathbf{x}) + \rho U_{ext}(\mathbf{x}). \tag{13}$$

The energy is divided into two parts. The internal field $U_{int}(\mathbf{x})$ favors specific spatial structures in the configuration $\mathbf{x}$, while the external field $U_{ext}(\mathbf{x})$ quantifies the quality of the configuration with

respect to the data. The positive parameter ρ allows the tuning of the relative weights between the two terms.

The simplest way of specifying a data term is to expand it as a sum over the objects in a configuration

$$U_{ext}(\mathbf{x}) = \sum_{u \in \mathbf{x}} U_d(u). \tag{14}$$

The definition of a data term for the whole configuration is thereby reduced to the definition of a data term for one object. The mapping $U_d(.)$ from S to $\mathbb{R}$ quantifies the relevance of an object with respect to the data. Note that a Bayesian modeling would result in a log-likelihood $-U_{ext}(\mathbf{x}|I)$ that has no reasons to be expandable over the objects.

If the data energy of an object u is negative ($U_d(u) \leq 0$), we say that the object is *attractive*. Care is needed to avoid superpositions of points. From equation (14) it is obvious that if $U_d(u) \leq 0$, then successive additions of clones of u decrease the overall data energy $U_{ext}(\mathbf{x} \cup u \cup u) \leq U_{ext}(\mathbf{x} \cup u) \leq U_{ext}(\mathbf{x})$. As a consequence, a repulsive term avoiding such superpositions is needed, and we eventually add an *exclusion* term $U_{excl}(\mathbf{x})$ to the energy

$$U(\mathbf{x}) = \rho \sum_{u \in \mathbf{x}} U_d(u) + U_{int}(\mathbf{x}) + U_{excl}(\mathbf{x}), \tag{15}$$

such that

$$U(\mathbf{x} \cup u \cup u) > U(\mathbf{x} \cup u), \quad \forall\, (u, \mathbf{x}) \in S \times \mathcal{C}.$$

2.3 Internal Field

The purpose of the internal field is to favor pre-defined patterns of objects. In the specific case of segments and rectangles, our purpose is to favor paving patterns of rectangles, connections of segments, and completion between rectangles and segments.

The simplest Gibbs point process with non-independent points is the *Strauss process*. Let consider a point process $\mathbf{X}$ in K describing random configurations of simple points

$$\mathbf{X}(\omega) = \{x_1, \ldots, x_{n(\mathbf{X}(\omega))}\}, \qquad x_i = (c_1^i, c_2^i) \in \mathbb{R}^2. \tag{16}$$

The Strauss process is based on the energy $U(\mathbf{x}) = \gamma s(\mathbf{x})$. The function $s(\mathbf{x})$ counts the number of pairs of points that are closer than a parameter δ while $\gamma > 0$ is a real parameter tuning the importance of the interaction term. In view of Equation (13) the Strauss process penalizes configurations with too many close points. Note that the process can alternatively be seen as a process of disks with radius $\delta/2$, and $s(\mathbf{x})$ counting the number of intersections between disks.

Strauss processes were originally introduced [24] for modeling patterns of trees, and the repulsive nature of the interaction was obviously suitable to that particular application. In our case, we would like to favor some clusters (e.g. segment connections). An naive solution would be to take a similar model and set $\gamma < 0$. However, in that case, the process is not defined ($Z = \infty$). The behavior of $s(\mathbf{x})$ is indeed in $n(\mathbf{x})^2$ (see [7] or [16] for details).

2.3.1 Definitions

For a given relation $\sim$ on S, let note $\mathcal{R}(\mathbf{x})$ the set of interacting couples of $\mathbf{x}$

$$\mathcal{R}(\mathbf{x}) = \{(u, v) \ : \ u \in \mathbf{x},\ v \in \mathbf{x},\ \ u \neq v \ \ u \sim v\}\,. \tag{17}$$

The relation $\sim$ can be symmetric, but it is not required. We define the neighborhood $\mathcal{N}(\mathbf{x}, u)$ of a point u in $\mathbf{x}$ as the set of points in $\mathbf{x}$ that are in relation with u

$$\mathcal{N}(u, \mathbf{x}) = \{v \in x \ : \ u \sim v\}. \tag{18}$$

Let consider the function

$$V(\mathbf{x}, u) = \mathbf{1}(\mathcal{N}(u, \mathbf{x}) \neq \emptyset) \tag{19}$$

which is null only if u has no neighbors in $\mathbf{x}$. This function is included in the model in order to favor or penalize the presence of an interacting pair of points.

We are also interested in ordering interactions with respect to a quality function. We suppose that for each type of interaction, a function $\Psi(.,.)$ from $S \times S$ to $[-1, 1]$ quantifies the quality of the interaction between interacting objects (loosely speaking, $\Psi(u, v)$ close to 1 (resp. -1) means "the interaction is good (resp. bad)" while $\Psi(u, v) = 0$ whenever (u, v) do not interact).

Care is needed with the incorporation of those Ψ functions in the configuration energy. Similarly to the attractive Strauss model, summing the Ψ values over the interacting couples would result in a non integrable $h(.)$. Again, since an object is possibly involved into several interactions, the number of interacting couples can evolve with a $n(\mathbf{x})^2$ behavior. As a consequence, we propose to compute for each object the maximum reward value

$$W(\mathbf{x}, u) = \begin{cases} \max_{v \in \mathcal{N}(\mathbf{x}, v)} \Psi(u, v) & \text{if } \mathcal{N}(\mathbf{x}, u) \neq \emptyset, \\ 0 & \text{otherwise.} \end{cases}$$

The function $W(u, \mathbf{x})$ is the reward function of the best interaction among those involving u. Note that for a repulsive interaction it might be better to compute the worst one (minimizing Ψ).

2.3.2 Local energies

We define the *local energy* of an object $u \in \mathbf{x}$ associated with a specific interaction to be a linear combination of the corresponding functions V and W,

$$u \in \mathbf{x}, \qquad U^{\sim}_{loc}(\mathbf{x}, u) = -\left(a^{\sim} V^{\sim}(\mathbf{x}, u) + b^{\sim} W^{\sim}(\mathbf{x}, u)\right). \tag{20}$$

Here a and b are two real parameters tuned to favor $(a, b > 0)$ or penalize $(a, b < 0)$ patterns of interest. As we already pointed it out, a favors the presence of an interacting object while b weights the quality of the best interaction involving u.

We finally define the total interaction energy of the configuration as the sum of local energies over the objects

$$U^{\sim}(\mathbf{x}) = \sum_{u \in \mathbf{x}} U^{\sim}_{loc}(\mathbf{x}, u). \tag{21}$$

2.3.3 Generalization

When using several interactions $\sim^1, \ldots, \sim^k$, we naturally extend the model by summing Equation (21) over the different interactions

$$\begin{aligned} U_{int}(\mathbf{x}) &= \sum_{i=1}^{k} U^i(\mathbf{x}) && (22) \\ &= \sum_{u \in \mathbf{x}} \sum_{i=1}^{k} U^i_{loc}(\mathbf{x}, u) && (23) \\ &= -\sum_{u \in \mathbf{x}} \sum_{i=1}^{k} [a^i V^i(\mathbf{x}, u) + b^i W^i(\mathbf{x}, u)]. && (24) \end{aligned}$$

The internal field accordingly evolves linearly with the number of points in the configuration. Combinatorial problems therefore disappear and the process is well defined. Another advantage is that the balance between the external field (data term) and the internal field is eased. A last and important benefit of this interaction model is its scale invariance. The weights a^i, b^i actually do not depend on the size of the considered area, provided that the density of objects to be detected is constant, a point we discuss in Section 4.

2.4 Exclusion Interaction

Although the attractive interaction model described previously solves the issue of the model integrability, an exclusion term penalizing redundant objects is needed. We already provided an immediate justification for this need through the discussion on the data term and the definition of attractive objects. It should also be noticed that attractive interactions enhance this need. Without an exclusion term, the density maximum can consist of an infinite accumulation of points, even if the density is integrable. A last reason for adding a repulsive interaction comes from a condition to the algorithm convergence (see [16]) which requires the energy variation induced by adding a point to be uniformly bounded.

These three reasons underline the need for an exclusion term. Since we consider geometrical objects, the simplest exclusion interaction we can use is the *intersection relation*

$$u \sim^{excl} v \quad \text{iff} \quad \text{Surf}(u) \cap \text{Surf}(v) \neq \emptyset \quad . \tag{25}$$

where we note by $\text{Surf}(u)$ the silhouette of the geometrical object u.

Associated energy To incorporate this interaction as a repulsive one, we use a simple model, homogeneous to the general interaction model of Equation (20)

$$U_{excl}(\mathbf{x}) = -a^{excl} \sum_{u \in \mathbf{x}}, V_{excl}(\mathbf{x}, u) \qquad a^{excl} < 0. \tag{26}$$

Here $|a^{excl}|$ is taken large enough so that it is impossible to have redundant objects in the maximizing configuration. However, due to the linear property of our attractive model, the exclusion weight does not need to be too large, resulting in good mixing properties of the algorithm.

2.5 Data term

In this section, we provide a generic analysis of the data term $U_d(u)$ associated with an object u.

Attractive objects. A data term $U_d : S \to \mathbb{R}$ partitions the set S into the set of attractive objects $U_d \leq 0$ and its complement (repulsive objects). Since the density h is maximized by a simulated annealing procedure, a repulsive object cannot be part of the resulting configuration, except if attractive interactions force its presence. For the sake of clarity, we avoid that phenomenon by considering attractive interactions among attractive objects only. We note $\gamma_1^r \subset S^r$ the set of attractive rectangles and γ_0^r its complement. Similarly the set of attractive segments is noted γ_1^s while the set of repulsive segments is noted γ_0^s.

Attractive object ordering. The function U_d allows the ordering of objects. We separate two cases. Among the repulsive objects, we use this function to favor repulsive objects close to the set of attraction γ_1 whereas for attractive objects we use $U_d(.)$ to favor the specific locations that fit the data the best.

3 Specific model dedicated to the analysis of DEMs

The purpose of this section is to present a specific model for the analysis of Digital Elevation Models. We define the rectangles and segments processes in terms of their internal field and data terms. We also present an interaction term to make both processes interact.

3.1 Segments and discontinuities

We enumerate in this section the different parts composing the segment model. We first explicit the data term, whose goal is to make the linear network match meaningful discontinuities of the DEM. We then describe the attractive connection interactions used along with the corresponding repulsive term. We conclude the section by presenting a simulated example of the action of the internal field on the segment process.

3.1.1 Configurations of segments

As mentioned in the previous section we consider a segment space S^s, product of the image K and the segment mark space $S^s = K \times M^s$

$$M^s =) - \frac{\pi}{2}, \frac{\pi}{2}] \times [L_{min}, L_{max}].$$

Points in $S^s = K \times M^s$ are segments parameterized by their center in the image together with their orientation and length. A marked point process $\mathbf{Y}$ on S^s describes random configurations of segments

$$\forall \omega \in (\Omega, \mathcal{A}, \mathbf{P}) \qquad \mathbf{Y}(\omega) = \{y_1, \ldots, y_{n(\mathbf{Y}(\omega))}\} \tag{27}$$

with $y_i \in S^s$, for all $i \in \{1, \ldots, n(\mathbf{y})\}$.

3.1.2 Data term

Our purpose is to use linear networks for detecting significant discontinuities on the DEM. Segment networks have previously been used in the context of road detection ([11], [23]). The aim of the data term is to quantify the relevance of a segment hypothesis with respect to the DEM. Since we want to process various type of DEMs, we propose to use the generic discontinuity detector that we presented in [17].

Discontinuity filter. Figures 3 and 4 provide a graphical explanation of our approach. For a given segment hypothesis, we consider slices taken orthogonally to the segment direction on the DEM. For each of these slices, the discontinuity filter detects discontinuity locations.

We use a dedicated filter. This filter is based on the accumulation of large enough gradients values, and permits the analysis of smooth data (e.g. Laser measurements), as well as sharper DEMs (e.g. provided by optical stereovision).

This detector relies on the following steps.

- First, on each profile, the points such that the gradient is larger than a parameter $\nabla H_{\min}$ are pre-selected.
- Second, the pre-selected gradients are accumulated, and selected if the accumulation is greater that ΔH_{min}.
- Finally, the discontinuity closest to the segment is kept as the important point.

A morphological opening step is also performed, using a linear element of size l_{sel}. A complete description of the filter is given in [14].

An important point is that this filter is implicitely directional as the slices analysis are performed orthogonally to a segment hypothesis.

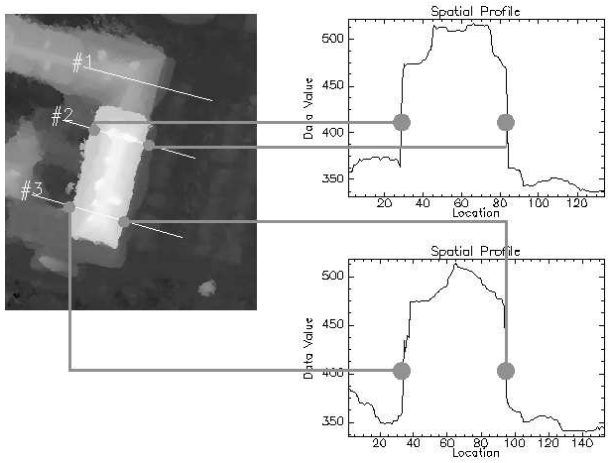

Figure 3: A Digital Elevation Model, some slices and the meaningfull discontinuities.

Reward functions. We detail here how the selected discontinuities are incorporated into the data term. As already discussed in the previous section, the data term $U_d(.)$ enables the discrimination between attractive and repulsive objects.

For a given segment hypothesis u on which the discontinuity analysis has been performed, we compute the length of detected discontinuity $Lg(u)$ as illustrated by the Figure 4(c). This length is given by the ratio of selected discontinuities, that are at a distance to the segment smaller than a parameter δr, multiplied by the length of the segment. We also compute a moment value, $\hat{m}(u)$, as illustrated by Figure 4(d). This moment is the average squared distance between the detected discontinuities and the segment.

Final data term. We define the set of attractive segments as the set of segments such that the ratio of detected discontinuities is greater than a fixed threshold $\eta \in [0, 1]]$

$$\gamma_1^s = \{u \in S^s \qquad \text{s.t. } Lg(u) \geq \eta L(u)\}$$

In practice, we take $\eta = 90\%$. As a consequence, the set of attractive segments is the set of segments lying on discontinuities. We also define a reward function $j_{seg} : S^s \to \mathbb{R}$ associated with a segment

$$j_{seg}(u) = \frac{1}{2}\frac{Lg(u)}{L_{max}} + \frac{1}{2}(1 - \hat{m}(u)).$$

This reward function favors segments with a large discontinuity length and fitting the discontinuities well. Therefore we get

$$U_d^s(u) = \left(-j_{seg}(u) * \mathbf{1}_{\gamma_1^s}(u) + 0.1 * (2 - j_{seg}(u))\mathbf{1}_{\gamma_0^s(u)}\right)$$

This data term favors the attractive segments and leads elements of γ_0^s towards the set of attractive elements γ_1^s as it associates low values with segments in good correspondence with the discontinuities of the DEM.

3.1.3 Internal field for the segment

We describe in this section the internal field designed to favor configurations of connected segments. We consider two different connection cases depending on the angle between the segments. We promote cases where the connection happens between aligned or orthogonal segments.

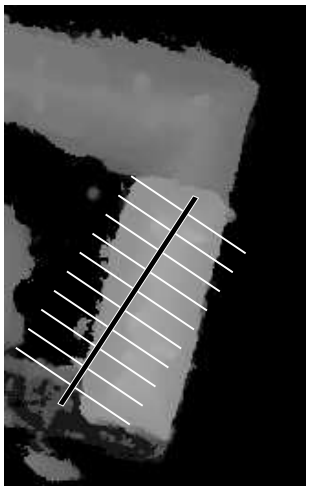

(a) A segment hypothesis (in black) on a Digital Elevation Model and the considered slices, orthogonal to the segment.

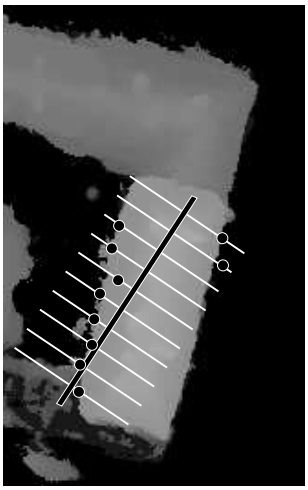

(b) We use a dedicated filter to detect on each slice the closest meaningfull discontinuity to the segment.

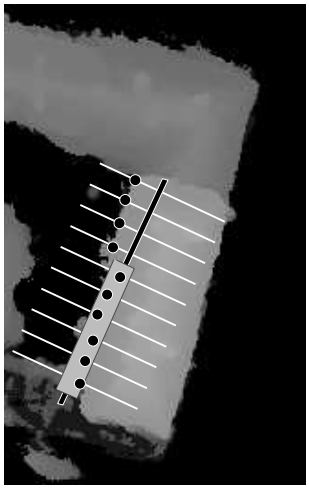

(c) The detected discontinuity length corresponds to the length of the gray rectangle.

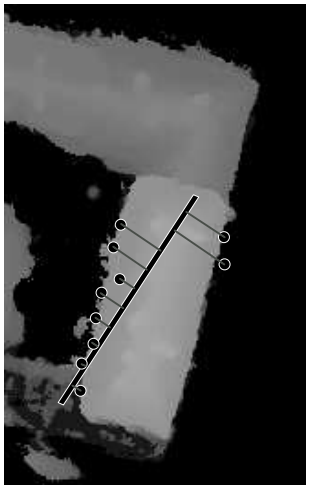

(d) The discontinuity moment is the average squared distance between the selected discontinuities and the segment.

Figure 4: Illustration of the steps used to compute the data energy of a segment hypothesis. First, orthogonal slices are extracted from the DEM (4(a)). Then, using a dedicated filter, on each profile the closest meaningfull discontinuity is detected (4(b)). The data energy is based on the two following functions: we consider the length of detected discontinuity, which corresponds to the ratio of discontinuities that are close enough to the segment multiplied by its length (4(c)); as well as the average squared distance between the discontinuities and the segment, a value that we call discontinuity moment (4(d)).

Connections. Connection interactions for segment processes has been considered in the works of [11] and [22]. We use similar geometrical interactions, but our generic model of attractive interactions presented in section 2.3 allows an easier incorporation of a quality term.

We introduce a connection relation $\sim_{conn}$ depicted by Figure 6(a). We identify by $E_1(u)$ and $E_2(u)$ the extremities of the segment u (see Figure 5). We consider that two segments are connected if the distance between their extremities is less than a parameter $\delta E_{\max}$

$$u \sim_{conn} v \Leftrightarrow \min\{\|E_i(u) - E_j(v)\| \quad i,j \in \{1,2\}^2\} \leq \delta E_{\max}$$

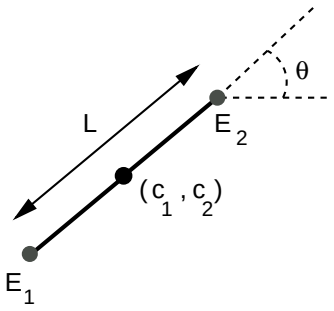

Figure 5: A segment, its parameterization and its two extremities.

Restrictions. We actually consider two different types of connections depending on the angle between the connected segments, and illustrated in Figure 6. We therefore append the following conditions on the difference of angles

$$\text{Cond1} \qquad \overset{\text{modulo } \pi}{|\ \theta(u) - \theta(v)\ |} \leq \delta\theta_{\max},$$

$$\text{Cond2} \qquad \overset{\text{modulo } \pi}{|\ \theta(u) - \theta(v) + \frac{\pi}{2}\ |} \leq \delta\theta_{max}.$$

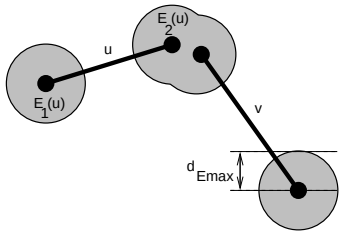

(a) Two connected segments

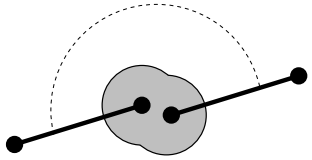

(b) A connection between aligned segments.

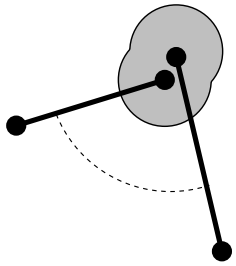

(c) A connection between orthogonal segments.

Figure 6: Connection interactions between segments. Two segments are connected if the distance between their extremities is small enough (6(a)). Two types of connections are actually distinguished: connections with a flat angle (6(b)) and connections with a right angle (6(c)).

We finally add a further restriction, and consider only connections between attractive segments. Since a segment has two extremities, we consider two relations of each type per segment, resulting in the following definitions:

$$u \sim^{\text{conn. al.}_1} v \quad \Leftrightarrow \quad \begin{cases} (u,v) \in \gamma_1^s \times \gamma_1^s \\ \min\{\|E_1(u) - E_1(v)\|, \|E_1(u) - E_2(v)\|\} \leq \delta E_{\max} \\ |\theta(u) - \theta(v)| \leq \delta\theta_{\max} \quad (\text{ modulo } \pi) \end{cases}$$

$$u \sim^{\text{conn. al.}_2} v \quad \Leftrightarrow \quad \begin{cases} (u,v) \in \gamma_1^s \times \gamma_1^s \\ \min\{\|E_2(u) - E_1(v)\|, \|E_2(u) - E_2(v)\|\} \leq \delta E_{\max} \\ |\theta(u) - \theta(v)| \leq \delta\theta_{\max} \quad (\text{ modulo } \pi) \end{cases}$$

$$u \sim^{\text{conn. orth.}_1} v \quad \Leftrightarrow \quad \begin{cases} (u,v) \in \gamma_1^s \times \gamma_1^s \\ \min\{\|E_1(u) - E_1(v)\|, \|E_1(u) - E_2(v)\|\} \leq \delta E_{\max} \\ |\theta(u) - \theta(v) + \frac{\pi}{2}| \leq \delta\theta_{\max} \quad (\text{ modulo } \pi) \end{cases}$$

$$u \sim^{\text{conn. orth.}_2} v \quad \Leftrightarrow \quad \begin{cases} (u,v) \in \gamma_1^s \times \gamma_1^s \\ \min\{\|E_2(u) - E_1(v)\|, \|E_2(u) - E_2(v)\|\} \leq \delta E_{\max} \\ |\theta(u) - \theta(v) + \frac{\pi}{2}| \leq \delta\theta_{\max} \quad (\text{ modulo } \pi) \end{cases}$$

3.1.4 Quality function

In order to favor good connections we introduce the following real valued function

$$\begin{array}{rccl} \varpi: & \mathbb{R}^2 & \to & [0,1] \\ & (x, x_{\max}) & \to & \dfrac{1}{x_{\max}^2}\left(\dfrac{1+x_{\max}^2}{1+x^2} - 1\right) \quad , |x| \leq x_{\max}. \end{array} \tag{28}$$

This function verifies $\varpi(0, x_{\max}) = 1$ and $\varpi(x_{\max}, x_{\max}) = 0$. In the case of the flat connection relation $\sim^{conn.al._1}$ we adopt the following reward function

$$\Psi(u,v) = \frac{1}{2}\varpi(\delta E(u,v), \delta E_{\max}) + \frac{1}{2}\varpi(\delta\theta, \delta\theta_{\max}).$$

where δE and $\delta\theta$ respectively represent the distance between the suitable extremities and the suitable angle difference. We therefore favor precise connections (the smaller the distance between the extremities, the better) as well as flat connections. The quality function associated with the orthogonal connection is similar and favors angle differences close to $\pi/2$.

Energy Model. We use the generic model presented in section 2.3. This model relies on four real parameters, $a^{\text{conn. al.}}, b^{\text{conn. al.}}, a^{\text{conn. orth.}}, b^{\text{conn. orth.}}$. As we want the connections to be favored, these parameters are taken positive. Note that since we have 4 connection relations, we should consider 4 couples (a, b). However, since the connections by one or another extremity is symmetric (relation $\sim^{\text{conn. al.}_1}$ equivalent to $\sim^{\text{conn. al.}_2}$) we set $a^{\text{conn. al.}_1} = a^{\text{conn. al.}_2} = a^{\text{conn. al.}}$ and proceed similarly for the other parameters.

3.1.5 Exclusion term.

Following the discussion in section 2.4 on the necessity of introducing a repulsive interaction to avoid accumulations of attractive points, we incorporate within the model an intersection interaction. For each segment, we define an embedding rectangle (see Figure 7) and set the exclusion interaction as the intersection between the corresponding rectangles.

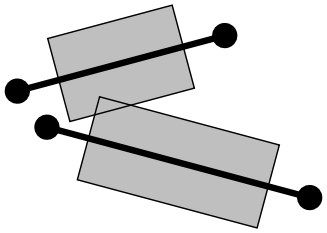

Figure 7: Two segments in repulsive interaction (the associated rectangles intersect).

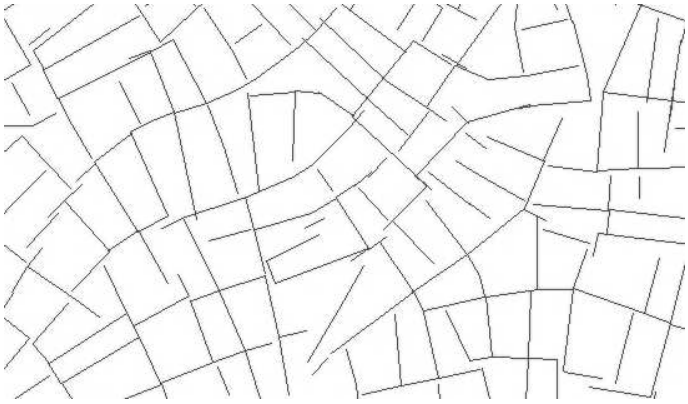

Figure 8: Simulation result of the internal field acting on the segment process.

3.1.6 Result example

We present on Figure 8 a simulation result of the prior model. The internal field favors connected networks of lines and both flat and orthogonal connections.

3.2 Rectangles and homogeneity

In this section we detail the rectangle process. After recalling the object space, we describe the data term as well as the internal field. We then show simulated results of the model.

3.2.1 Configurations of rectangles

We define a process of rectangles $\mathbf{X}$ whose points represent rectangles. The object space is $S^r = K \times M^r$.

$$M^r =]-\frac{\pi}{2}, \frac{\pi}{2}] \times [L^r_{min}, L^r_{max}] \times [l^r_{min}, l^r_{max}].$$

3.2.2 Rectangles and DEM

The goal of the data term is to make the rectangles fit extruded areas of the Digital Elevation Model. For that purpose we use a mask of points presented on Figure 9(a). This mask is made of a set of points inside a rectangle along with four bands around it.

Local ground height. We compute a local ground height estimate $\hat{H}_g(u)$ from the four bands. We take the minimum of the four means of heights. This procedure provides a local estimate of the ground height. This point is important, as dense urban areas often exhibit different "ground levels".

Extruded ratio. We define the volume ratio $\bar{v}(u)$ as the percentage of points inside the rectangle that are higher than the ground height estimate augmented by a minimum height $(\hat{H}_g(u) + H_{min})$.

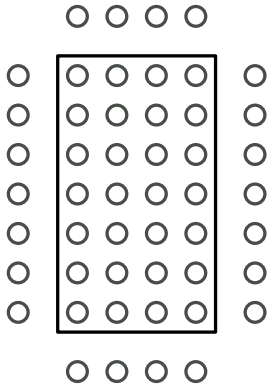

(a) A mask of points, associated with each rectangle, is made of a set of central points and four bands along the sides.

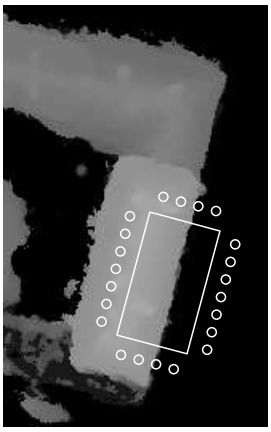

(b) The four bands are used to obtain a ground height estimate taken as the lowest average height among the four bands.

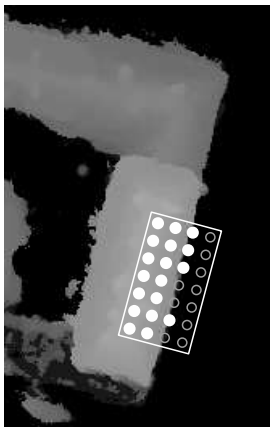

(c) The extruded ratio is given by the ratio of inside points higher than the ground height estimate augmented by a minimum height (points in white).

Figure 9: To compute the data energy of a rectangle we use a mask of points associated with the rectangle (9(a)). The four lateral bands gives four mean DEM height (9(b)). The lowest mean gives a local estimate of the ground height. We then compute a volume ratio (9(c)) that corresponds to the ratio of inside points that are higher than the ground height augmented by a minimum height, set by the user. We also compute the standard deviation of these points.

Surface ratio. Another function we use is the ratio between the area of the rectangle and the maximum possible area.

$$\tilde{s}(u) = \frac{l(u) * L(u)}{L_{\max} * l_{\max}}.$$

This function is included in the data term to favor large rectangles. It should be noted that a term favoring large rectangles could be considered as a part of the internal field.

Standard deviation ratio. We compute the standard deviation $\sigma(u)$ of grey levels among the points of the mask that are higher than the minimum height $\hat{H}_g(u) + H_{min}$. The standard deviation ratio is given by

$$\bar{\sigma}(u) = \max\left\{0, 1 - \frac{\sigma(u)}{\sigma_{\max}}\right\}.$$

This term obviously favors an homogeneous distribution of gray levels inside the rectangles. Note that this term relies on an additional parameter $\sigma_{\max}$, which in practice we take as $\sigma_{\max} = 10m$.

3.2.3 Data term

Attractive objects. We define the set of attractive rectangles as the set of rectangles for which the extruded ratio is large enough

$$u \in \gamma_1^r \Leftrightarrow \bar{v}(u) \geq v_{min}. \tag{29}$$

In practice, we use $v_{min} = 90\%$ and $H_{min} = 4m$.

Data function U_d. We consider the following reward function associated with a rectangle

$$j_{rect}(u) = \frac{1}{2}\bar{v}(u) * \bar{s}(u) + \frac{1}{2}\bar{\sigma}(u).$$

By multiplying the extruded and surface ratios, we actually obtain the surface of the rectangle that is above $\hat{H}_g(u) + H_{min}$. This function favors large homogeneous rectangles. We finally end up with the following data term

$$U_d^r(u) = \left(-j_{rect}(u) * \mathbf{1}_{\gamma_1^r}(u) + 0.1 * (2 - j_{rect}(u))\mathbf{1}_{\gamma_0^r(u)}\right)$$

Again, this function $U_d^r(.)$ discriminates between attractive and repulsive objects and favors the best objects, in the sense of the homogeneity of gray levels.

3.2.4 Internal field for the rectangle process

In a town, buildings are usually aligned. Hence, we design an interaction that favors such alignments. Figure 10(a) presents an example of alignment, while Figure 10(b) illustrates the different values used for the definition an alignment. This model is similar to the model we propose in [17].

Alignment interaction. Denoting $\delta C(u, v)$ the distance between appropriate corners and $\delta\theta(u, v)$ the angle difference between the two rectangles (modulo π), we define the first interaction by the three following conditions

$$u \sim^{al_1} v \quad \Longleftrightarrow \quad \begin{cases} \delta C(u, v) \leq \delta C_{\max} \\ \delta\theta(u, v) \leq \delta\theta_{\max} \\ (u, v) \in \gamma_1^2. \end{cases} \tag{30}$$

Because a rectangle has four corners, we actually define four different alignment interactions that we note $\sim^{al_1}, \ldots, \sim^{al_4}$. We only detect alignments between two attractive objects (belonging to γ_1^r). A

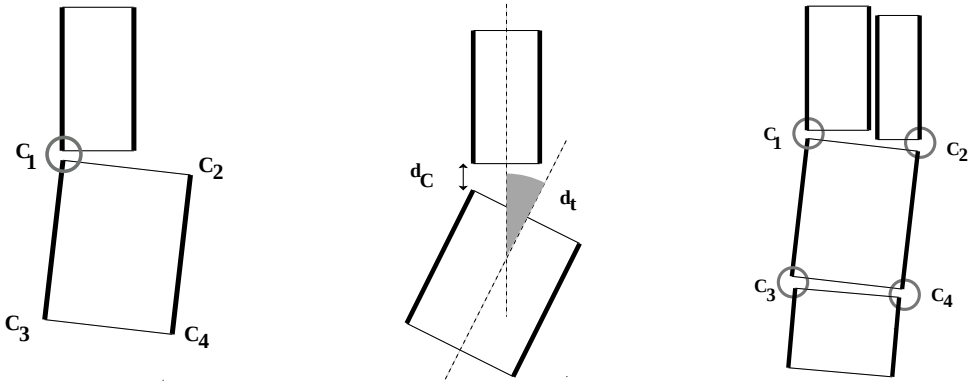

(a) Example 1 (b) Definition (c) Example 2

Figure 10: Alignment interactions. a) example of a single alignment, b) values needed to define an alignment and c) example of a rectangle interacting with three neighbors.

Figure 11: Illustration of the paving interactions.

rectangle can be in relation with a neighbor by two corners in which case we consider that they are related by two different interactions. Figure 10(c) shows an example of a rectangle that is related to three neighbors under the 4 alignment relations. The associated reward function evaluated on a couple of related points is:

$$\Psi(u,v) = \frac{1}{2}\varpi\left(\delta\theta(u,v), \delta\theta_{\max}\right) + \frac{1}{2}\varpi(\delta C(u,v), \delta C_{\max}\Big). \tag{31}$$

This reward function is important: the goal is not only to promote the presence of alignments, but also to favor alignments of good quality. We finally define the internal field

$$U_{int}(\mathbf{x}) = \sum_{u\in x} a^{al} \sum_{i=1}^{4} V^{al_i}(\mathbf{x}, u) + b^{al} \sum_{i=1}^{4} W^{al_i}(\mathbf{x}, u). \tag{32}$$

Note that although 4 alignment relations are considered, we only use two parameters a and b to limit the number of parameters.

Paving interaction. We also introduce a second type of relation which favors parallel rectangles that are located side by side as illustrated by Figure 11. This interaction is essentially introduced in order to favor clean arrangements of buildings. This relation is defined similarly to the alignment relation previously described. The reward function Ψ is also defined in a similar way. It leads to interactions $\sim^{pav_1 1}$ to $\sim^{pav_4}$.

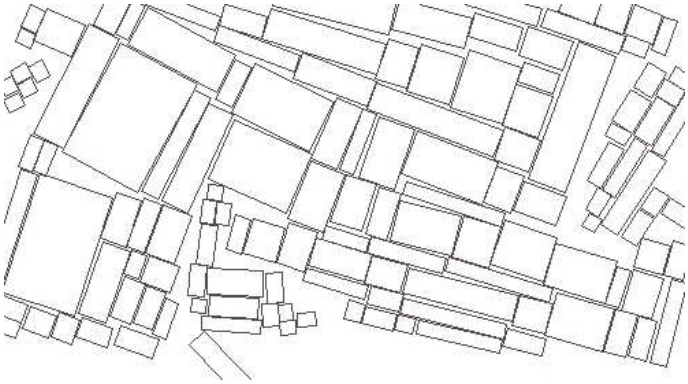

Figure 12: Simulation result showing of the internal field of the rectangle process.

3.2.5 Results

An illustrative example of a simulation of the internal field is presented on Figure 12.

3.3 Coopeeration between segments and rectangles

We present in this section an interaction between segments and rectangles whose purpose is to merge the two processes in order to obtain a joint analysis of the data based on both discontinuities and extruded area detection.

3.3.1 Union of point processes

We formally denote configurations of rectangles and segments as realizations of a process $\mathbf{Z}$, union of the processes $\mathbf{X}$ of rectangles and $\mathbf{Y}$ of segments

$$\mathbf{Z} = \mathbf{X} \cup \mathbf{Y}. \tag{33}$$

Alternatively, the point process $\mathbf{Z}$ can be seen as a marked point process on

$$S^{sr} = K \times ((\{s\} \times M^s) \cup (\{r\} \times M^r))) . \tag{34}$$

An object z is accordingly described by a point, an indicator $o \in \{s, r\}$, and the relevant marks. This alternative representation is useful from the algorithmic point of view, as it allows us to extend the convergence results we obtained in [17] and [16] to the case of a process of rectangles and segments.

3.3.2 Interaction between segments and rectangles

We define an interaction term between rectangles and segments in order to favor the coherence between the two networks of objects. We expose on Figure 13(a) the geometrical values computed to investigate wether a segment and a rectangle interact. We use a test on the angle difference, as well as a test on the distance between the segment center and the closest side of the rectangle. The associated limit parameters are noted $\delta d_{\max}$ and $\delta\theta^{rs}$.

Similarly to the previously defined interactions, we consider only interactions among attractive objects. Note that a segment can be in relation with two rectangles (two sides) while a rectangle can be related to four segments, as illustrated by the Figure 13(b).

We end up with the following interaction energy

$$U_{coop}(\mathbf{z}) = \sum_{u \in z} a^{coop} V(\mathbf{z}, u) + b^{coop} W^{coop}(\mathbf{z}, u). \tag{35}$$

where a^{coop}, b^{coop} are the interactioin parameters, and V, W the interaction functions defined similarly to the previous interactions.

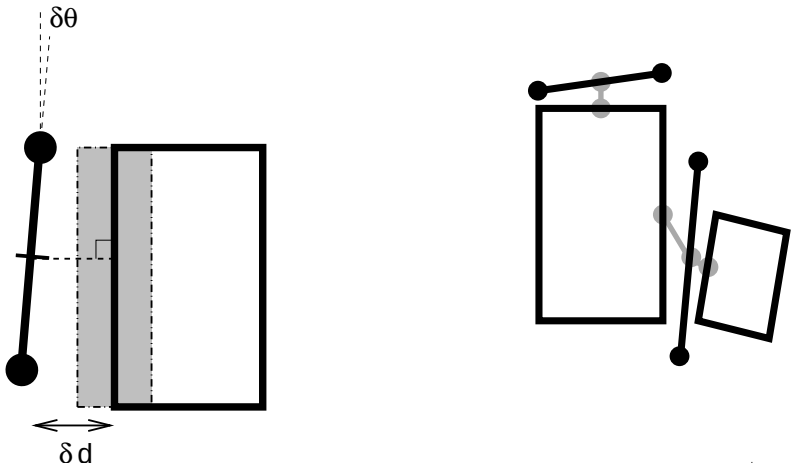

(a) A rectangle and a segment interact if the center of the segment lies inside the grey area and if the angle difference is lower than a threshold.

(b) Example of two rectangles interacting with two segments.

Figure 13: Illustration of the interaction between rectangles and segments.

3.3.3 Resulting model

Accounting for both the segment and rectangle processes result in the overall model

$$\begin{aligned} U^{rs}(\mathbf{z}) &= U^r(\mathbf{x}) + U^s(\mathbf{y}) + U^{inter}(\mathbf{z}) \\ &= \rho^r \sum_{u \in \mathbf{x}} U_d^r(u) + \rho^s \sum_{v \in y} U_d^s(v) + U_{int}^r(\mathbf{x}) + U_{int}^s(\mathbf{x}) + \dots \\ &\qquad \dots U_{excl}^r(\mathbf{x}) + U_{excl}^s(\mathbf{y}) + U_{coop}(\mathbf{z}) \end{aligned}$$

parameterized by ρ^r, ρ^s together with the a^i and b^i covering the two types of segment connections, the two types of rectangle alignment relations, the two repulsive interactions and the cooperation interaction.

4 Algorithm

We present briefly in this section the algorithm used for optimizing the model described by Equation (15). Rather than detailing technical issues that can be found in [7] or [16] we try to give a general flavor of the MCMC sampler we use.

4.1 Sampling unnormalized densities

As stated in section 2, we specify point process models by means of an energy $U(.)$ and a reference Poisson point process playing the analog role of real p.d.f. and Lebesgue measure for real random variables. The resulting distribution is denoted $\pi(.)$ and is known *up to a normalizing constant*. Due to the Markov Random Field approaches, it is now widely known in the image processing community that Gibbs or Metropolis-Hastings procedures allow the computation of Monte Carlo estimators, even

if the normalizing constant of the target distribution is not known. Such algorithms are Monte Carlo Markov Chain samplers generating Markov chains that exhibit the desired properties (i.e. Harris recurrence, aperiodicity, π invariance and ergodicity). As a consequence of these properties, the states of the Markov chain after a large enough time are distributed according to the desired distribution $\pi(.)$ and can be used to compute Monte Carlo values even if the samples are not independent, regardless of the starting point. Of course, mild conditions on the function to evaluate need to be fulfilled (e.g. it has to verify Lyapunov stability conditions, see [7]).

The point process case can be tackled similarly, by employing a Metropolis-Hastings like procedure. However, as it was pointed out by Green [8], when exploring state spaces of different dimensions, a correcting term has to be appended to the acceptance ratio when the Markov chain jumps between spaces of different dimensions.

As we now detail it, the Metropolis-Hastings-Green procedure applied to point processes is very similar to the usual Metropolis-Hastings update scheme. The transition kernel of the Markov chain is a two stage procedure. A possible new state is first randomly proposed by a perturbation kernel (*proposition step*) and then randomly accepted according to a suitable Bernoulli scheme (*acceptance step*). In the case of point processes, the current state is a configuration of geometrical objects. The random proposition can be for instance the translation or the rotation of one or several objects in the configuration or the addition/deletion of an item to/from the current configuration. In the latter case, the Green correcting factor is needed, since the dimension of the configuration is changed. The second step (random acceptation of the proposition) is the step that ensures the convergence of the Markov Chain to the desired distribution and the acceptance probability needs to be computed carefully.

The Metropolis-Hastings-Green algorithm applied to the specific case of point processes is known under the name of Geyer and Møller algorithm by the point process community since they provided a proof of its convergence in 1994.

4.2 Generic Structure

Suppose we consider a point process $\mathbf{Z}$ defined by its energy $U(.)$. Through the Gibbs relation, this energy leads to a density h known up to a normalizing constant. This density together with the distribution $\mu(.)$ of the reference Poisson point process defines the distribution $\pi(.)$ of $\mathbf{Z}$.

The Markov chain $(X_t)_{t\geq 0}$ is defined by a starting point $X_0 = \{\emptyset\}$ and a Markovian transition kernel $P(\mathbf{z}, .)$ corresponding to the conditional distribution of $X_{t+1}|X_t = \mathbf{x}$. It results in a Markov chain $(X_t)_{t\geq 0}$ on the space of finite configurations of points $\mathcal{C}$.

Of course, $P(.,.)$ is designed in order to make the Markov Chain converge towards the desired distribution.

$$\|P^n(\{\emptyset\}, .) - \pi(.)\|_{TV} \to 0 \tag{36}$$

where $\|.\|_{TV}$ notes the Total Variation norm (TV).

The Markov chain generated by the following algorithm satisfies this property. We actually have more accurate results, since we know that we can start from any configuration (Harris recurrence) and that the total variation tends to zero geometrically (geometric ergodicity), as detailed in [16].

4.2.1 Algorithm

The algorithm is based on a mixture of perturbation kernels $Q(.,.) = \sum_m p_m Q_m(.,.)$ where $\sum p_m = 1$ and $\int Q_m(\mathbf{z}, \mathbf{z}')\mu(d\mathbf{z}') = 1$. The algorithm iterates the following steps. We fix the current state X_t as $X_t = \mathbf{z} = \{z_1, \ldots, z_n\}$.

[1] Choose one of the proposition kernels $Q_m(.,.)$ with probability $p_m(\mathbf{z})$ and

[2] sample $\mathbf{z}'$ according to the chosen kernel $\mathbf{z}' \sim Q_m(\mathbf{z}, .)$.

[3] Compute the Green's ratio $R_m(\mathbf{z}, \mathbf{z}')$, function of the selected kernel Q_m, the original state $\mathbf{z}$ and the proposed new state $\mathbf{z}'$. The ratio R_m is derived to make the Markov chain converge towards the desired distribution.

[4] The proposition is accepted $X_{t+1} = \mathbf{z}'$ with a probability $\alpha_m(\mathbf{z}, \mathbf{z}') = min(R_m(\mathbf{z}, \mathbf{z}'), 1)$ and rejected otherwise $X_{t+1} = \mathbf{z}$.

4.2.2 Perturbation kernels

The efficiency of the algorithm highly depends on the variety of possible transformations $Q_m(\mathbf{z}, .)$.

Birth or death. This kind of perturbation first chooses with probability p_b and $p_d = 1 - pb$ wether a point should be removed (death) or added (birth) to the configuration. If death is chosen, the kernel selects randomly one point u in $\mathbf{z}$ and proposes $\mathbf{z}' = \mathbf{z} \setminus u$, while if birth is chosen, it generates a new point u according to the uniform measure $|.|/|S|$ and proposes $\mathbf{z}' = \mathbf{z} \cup u$. The birth or death kernel is necessary and sufficient to insure the convergence of the Markov chain towards the target distribution.

Non jumping transformations. Non jumping transformations are transformations that first select randomly a point u in the current configuration and then propose replacing this point by a perturbed version v, $\mathbf{z}' = \mathbf{z} \setminus u \cup v$. Translation, rotation or dilation are examples of non jumping perturbations.

Birth or death in a neighborhood. We introduced this kind of transformation in [16]. The idea is to propose the removal or addition of interacting pairs of points with respect to one of the attractive relations such as the connection in the case of segments or alignment in the case of rectangles.

Green ratio. With each of these proposition kernels a mapping $R_m(.,.)$ from $\mathcal{C} \times \mathcal{C}$ to $(0, \infty)$ is associated. This value, named *Green ratio*, depends on the target distribution π.

4.2.3 Simulated annealing

To find a minimizer of the energy $U(.)$ we use a simulated annealing framework. Instead of generating samples of $h(.)$, we simulate $h^{\frac{1}{T_t}}(.)$. The temperature parameter T_t tends to zero as t tends to ∞. Note that it is equivalent to the notation

$$f_t(\mathbf{z}) = Z_{T_t}^{-1} \exp\left(-\frac{U(\mathbf{z})}{T_t}\right). \tag{37}$$

This technique has been widely used in image processing (see [28] for instance). If T_t decreases with a logarithmic rate, then X_t tends to one of the global maximizers of $h(.)$. Of course, in practice it is not possible to use a logarithmic evolution law and we eventually use a geometrical one. This last point makes the quality of the proposition kernels an important issue. As a consequence we design kernels such that the trajectory of the Markov chain is poorly correlated to insure a good exploration of the state space.

4.3 Specific Transformations

We detail in this section the proposition kernels used in our case.

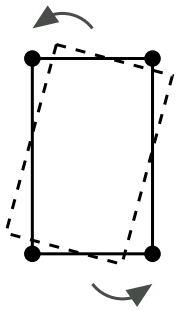

(a) Rotation of a rectangle.

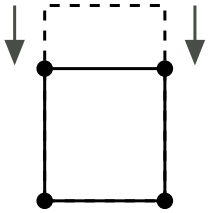

(b) Rectangle dilation in one direction.

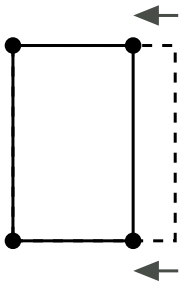

(c) Rectangle dilation in the second direction.

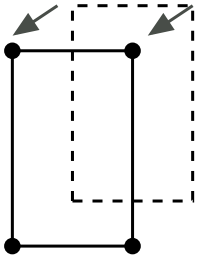

(d) Rectangle translation.

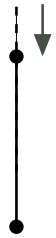

(e) Segment dilation.

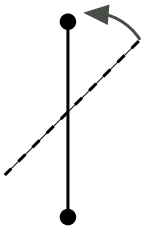

(f) Segment rotation.

(g) Segment translation.

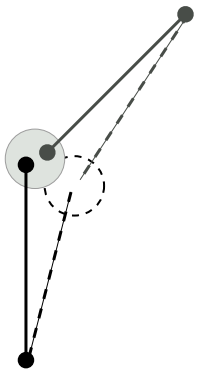

(h) Modification of the connection between two connected segments.

Figure 14: The different non jumping transformations used in the algorithm. Each of these transformations first randomly selects an object in the current configuration of rectangles and segments and applies a specific parameter perturbation on the selected object, except in the case of a connection perturbation (14(h)) where two objects are modified.

4.3.1 Birth or death transformations

We consider two simple birth or death transformations, Q_{BDR} and Q_{BDS} corresponding to the random birth or death of a rectangle (BDR) or a segment (BDS). The birth update follows a uniform distribution $|.|/|S^r|$ or $|.|/|S^s|$ depending on the type of object to create. The death update proposes removing an object uniformly selected among the current objects. The Green ratios associated with the birth and the death of a rectangle are respectively

$$R_{BDR}(\mathbf{z}, \mathbf{z} \cup u) = \frac{|S^r|}{n(\mathbf{z})+1} \frac{h(\mathbf{z} \cup u)}{h(\mathbf{z})}, \qquad R_{BDR}(\mathbf{z}, \mathbf{z} \setminus u) = \frac{n(\mathbf{z})}{|S^r|} \frac{h(\mathbf{z} \setminus u)}{h(\mathbf{z})}. \tag{38}$$

The ratios in the case of birth or death of a segment are similar.

4.3.2 Translations, rotations, dilatations

We have implemented the transformations depicted in Figure 14. Each of these transformations uses a parameter z that is randomly chosen in some symmetric set Σ. For instance, the rotation perturbations use a random parameter $\xi \in \Theta = [-\Delta\varphi, \Delta\varphi]$ to generate the new angle for the selected object. If u is chosen uniformly in $\mathbf{z}$ and the distribution of ξ is symmetric, the suitable Green ratio is given by the usual Metropolis-Hastings ratio

$$R(\mathbf{z}, \mathbf{z}') = \frac{h(\mathbf{z}')}{h(\mathbf{z})}. \tag{39}$$

4.3.3 Birth or death of an aligned rectangle

This kernel proposes either to create (with probability p_b) or to remove (with probability $p_d = 1 - p_b$) an interacting pair of rectangles.

Birth. The birth update first selects a point u of $\mathbf{z} \cap \gamma_1^r$, then generates a new point v aligned with u in the sense of one of the alignment relations $\sim^a l$, and proposes $\mathbf{z}' = \mathbf{z} \cup v$.

Death. The death update selects a pair of aligned points provided that at least one of them is in γ_1^r, chooses an object v in this pair with probability 0.5, and proposes to remove v: $\mathbf{z}' = \mathbf{z} \setminus v$.
The expression for the Green ratio associated with this kind of transformations is detailed in [16] and [17], and we refer the reader to these papers for detailed explanations on how the ratios were derived.

4.3.4 Connexions perturbation

This intuitive transformation allows to modify the segment network, by acting simultaneously on two connected segments. The different steps are

`[1]` choose a couple of connected segments,

`[2]` generate a random perturbation vector,

`[3]` apply this vector to each of the connected extremities ,

`[4]` test if the two new segments are still connected, if not stop here, otherwise

`[5]` propose $\mathbf{y}'$ obtained by replacing the two former segments by the new perturbed one.

This transformation is illustrated by Figure 14(h). The Green ratio is given by $h(\mathbf{z}')/h(\mathbf{z})$.

4.4 Reference measure

4.4.1 Comments

For computational convenience, the reference intensity measure $\nu(.)$ usually used is uniform ([26]). This intensity measure defines the reference Poisson point process distribution $\mu(.)$. Let consider

$$\nu(.) = |.|_K \times \frac{|.|_M}{|M|} \tag{40}$$

It describes a homogeneous Poisson point process that puts on average $|K|$ objects in S. Interestingly, the configuration maximizing $h(\mathbf{z})$ does not depend on the chosen reference measure. The advantage of using a simple intensity measure is that it makes the birth of a point easier. For instance, using Equation (40) implies that the birth step uses a uniform generation over S. However, in our setup, points of interest are those in γ_1 which is of small Lebesgue measure. To improve the exploration of γ_1, a solution is to use a reference measure favoring this set. It is possible to do so and keep the nice uniform generation. The solution is to add a "measure term" to the energy :

$$h(.) \propto \exp\left(\sum_{u\in\mathbf{z}} \log(\beta(u)) - \frac{U_{int}(\mathbf{z}) + U_{excl}(\mathbf{z}) + \rho U_{ext}(\mathbf{z})}{T}\right). \tag{41}$$

This is equivalent to changing the reference intensity measure, except that it permits to keep the computationally simple uniform generation. We denote by $\nu'(.)$ the corresponding reference measure, given by equation (10).

4.4.2 Utility of the partition

As detailed in section 2, we have defined a partition of S as $S = \gamma_1^r \cup \gamma_0^r \cup \gamma_0^s \cup \gamma_1^s$. We propose to use the following function β:

$$\log \beta(u) = \sum_{o\in\{r,s\}} \sum_{i\in\{0,1\}} \log(\beta_i^o)\mathbf{1}(u \in \gamma_i^o), \tag{42}$$

resulting in the following property :

$$E_i^o = \mathbb{E}[N_{\gamma_i^o}(\mathbf{Z})] = \nu'(\gamma_i^o) = \beta_i^o \nu(\gamma_i) = \beta_i^o |K| \frac{|\gamma_i^o|}{|S|}. \tag{43}$$

We tune the weights such that the E_i^o's are of the same order, making all γ_i^o approximatively equivalent with respect to the exploration ability of the Markov chain. Another advantage of this parameterization is its independence to the observed area K, since $\nu'(.)$ is proportional to the surface measure (Lebesgue measure in $\mathbb{R}^2$). Using an MCMC run, we compute the values $|\gamma_i^o|/|S|$ and then set the β_i^o values such that

$$E_i^o \approx |K|$$

where $|K|$ corresponds to the area, in meters squared, of the urban zone under consideration.

4.5 Convergence of the algorithm

The convergence of the algorithm holds. We derived sufficient conditions in [16] and showed in [17] that these conditions are fulfilled in the specific case of a process of rectangles. The generalization to the case of processes of both segments and rectangles is straightforwad, due to the representation of Equation (34).

The convergence of the simulated annealing towards a global maxima of the density $h(.)$ has been proved in [25] using Dobrushin conditions.

Rectangle space	
$l^r_{\min}$	5m
$l^r_{\max}$	30m
$L^r_{\min}$	5m
$L^r_{\max}$	40m

Segment space	
$L^s_{\min}$	9m
$L^s_{\max}$	30m

Table 1: Space parameters

Rectangle model parameters	
Interaction definition	
$\delta C_{\max}$	6m
$\delta\theta^r_{\max}$	30°
Alignments	
$a^{\sim^{al}}$	0.3
$b^{\sim^{al}}$	0.4
Paving relation	
$a^{\sim^{pav}}$	0.3
$b^{\sim^{pav}}$	0.4
Exclusion parameter	
$a^{\sim^{excl}}$	-10

Segment parameters	
Interaction definition	
$\delta E_{\max}$	$5m$
$\delta\theta^s_{\max}$	30°
Flat connection	
$a^{\sim^{conn.al.}}$	1.5
$b^{\sim^{conn.al.}}$	1.5
Orthogonal connection	
$a^{\sim^{conn.orth.}}$	0
$b^{\sim^{conn.orth}}$	2
Exclusion relation	
$a^{\sim^{excl.s}}$	-15

Cooperation	
Interaction definition	
$\delta d_{\max}$	6m
$\delta\theta^{rs}_{\max}$	30°
Weights	
$a^{\sim^{coop.}}$	0.1
$b^{\sim^{coop.}}$	1

Table 2: Parameters describing the internal field of both processes as well as the interaction term between rectangles and segments. These parameters are fixed for all the results presented in this section.

5 Results

We present in this section a set of results on real data. We first detail the parameters of the internal field, as these parameters were fixed once for all and applied to all results.

We then present results on a very crude DEM. This example illustrates how interesting it is to include two different type elements. We first present a result obtained using only a process of segments, then a result obtained using only a process of rectangles and finally a result obtained using both processes.

We then present results on different type of data, showing the generality of the proposed model.

5.1 Fixed parameters

On Table 1 we present the space parameters, while on Table 2 we present the parameters defining the internal model. These parameters are fixed for all the results presented later in the section. These parameters have been tuned by hand, but a supervised learning is possible, if some examples are provided (see [7]).

5.2 Very crude DEM

5.2.1 Presentation

We present in Figure 15 a very crude Digital Elevation Model. This DEM comes from a simulation and has been provided to us by the French National Geographic Institute (IGN). We consider this DEM to be very crude as it exhibits two main characteristics. First, due to the way the data have been generated, the vertical resolution of the DEM is very low, as shown by the low number of gray

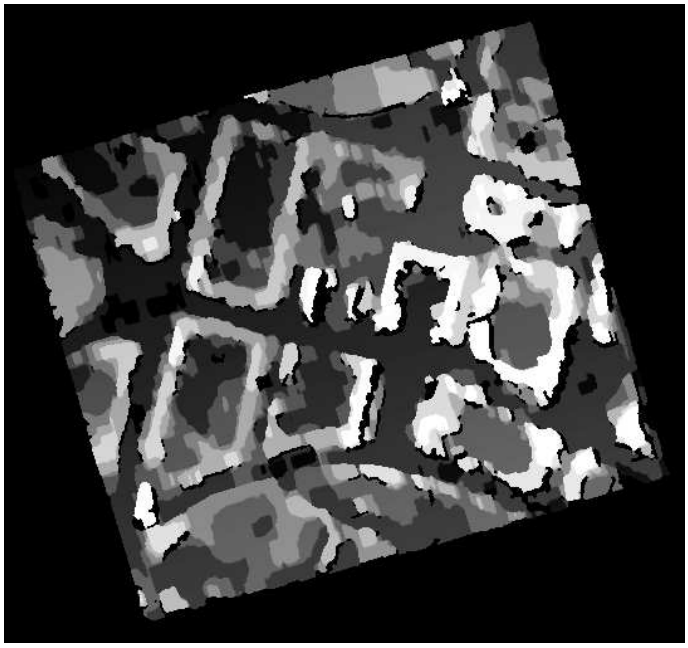

Figure 15: Crude Digital Elevation Model provided by the French National Geographic Institute (©IGN). The analysis of this DEM faces two major issues: first, large areas of data are missing (black areas); second, the vertical resolution is poor, limiting the amount of information available.

Rectangular mask	
Inside points resolution	2m
Distance of lateral bands	110m

Rectangle data term parameters	
$H_{\min}$	5m
$v_{\min}$	90%
$\sigma_{\max}$	5m

Rectangle data term weight	
ρ^r	1.2

Slices parameters	
Slices discretization step	1m
Distance between slices	2m
Length of slices	30m

Segment data term parameters	
$\nabla H_{\min}$	0.7
$\delta H_{\min}$	5
l_{sel}	4m
δ_r	8m
η	90%

Segment data term weight	
ρ^s	3

Table 3: Rectangle and segment data term parameters.

levels of Figure 15. Second, there are some occlusions: large amounts of data represented by black areas are missing.

5.2.2 Rectangles process

Model Parameters. We present on Table 3 the data term parameters employed. In addition to the definition of attractive rectangles presented in Equation (29) we consider a rectangle to be attractive if the amount of data available is large enough (at least 70% of the rectangle surface).

Results. We present on Figure 16 a detection result obtained by using only the rectangle process. The homogeneity data term clearly plays its role. The segmentation obtained indeed follows the homogenous areas. However, the rectangles fail to follow the discontinuities.

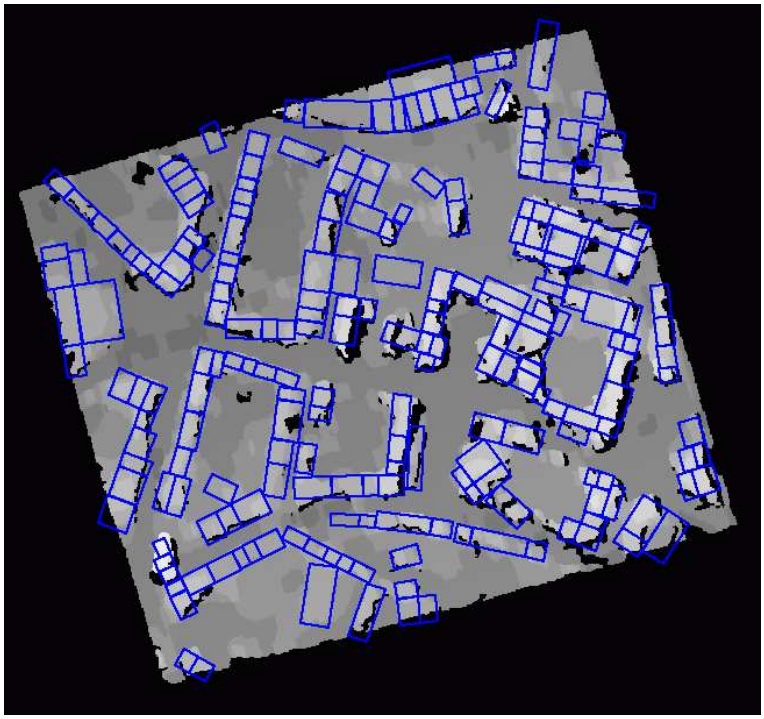

Figure 16: Extraction result obtained by using the process of rectangle only.

5.2.3 Segments process

Segment parameters. We present the segment data term parameters in Table 3. These parameters were tuned to deal with smooth discontinuities.

Results. On Figure 17, we present an extraction result obtained using the segment process only. Note that the extraction process tends to give curved linear networks.

5.2.4 Cooperation between segments and rectangles

Results We present the extraction result obtained by using the two processes together in two steps. On Figure 19, we show the obtained segment configuration, while on Figure 18 we show the rectangle configuration.

The cooperation term plays its role, as both the rectangles and the segments processes fit the data better when used together. This example on a crude DEM is however disappointing. The data is indeed too crude to obtain a satisfactory extraction result, although it illustrates well the originality of our approach. As a consequence, we present in the rest of this section results on different Digital Elevation Models.

5.3 Satellite DEM

We present on Figure 20 another simulation of a satellite DEM also provided by the IGN. This DEM is far better and the rectangle extraction is therefore more meaningfull. We present in Table 4 the data term parameters employed.

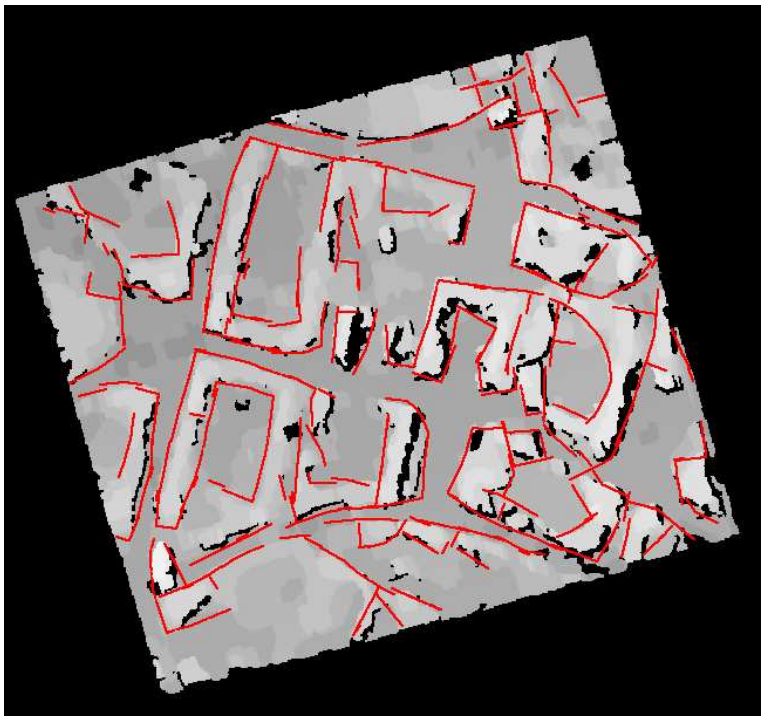

Figure 17: Extraction result obtained by using the segment process only.

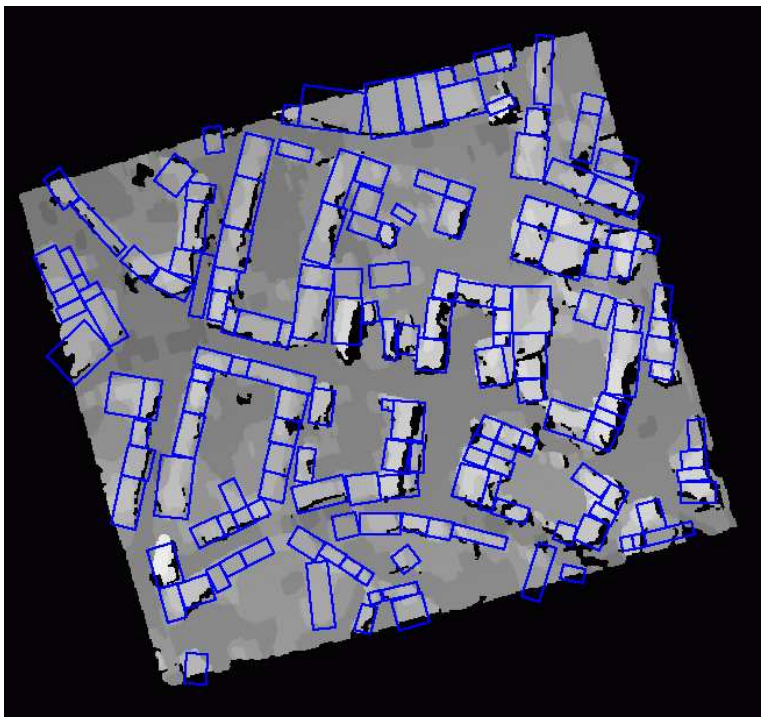

Figure 18: Rectangle extraction result obtained using both processes simultaneously.

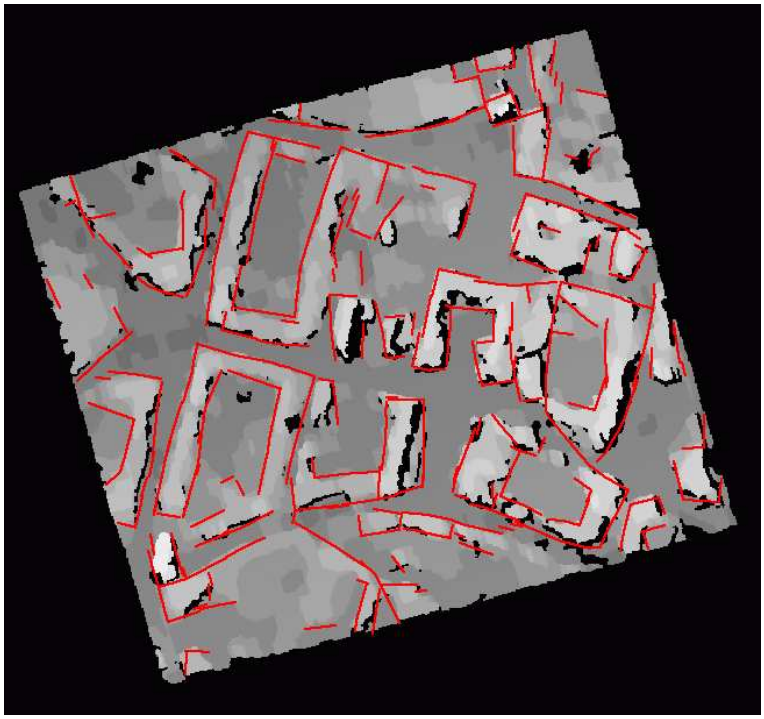

Figure 19: Segment extraction result obtained using both process simultaneously.

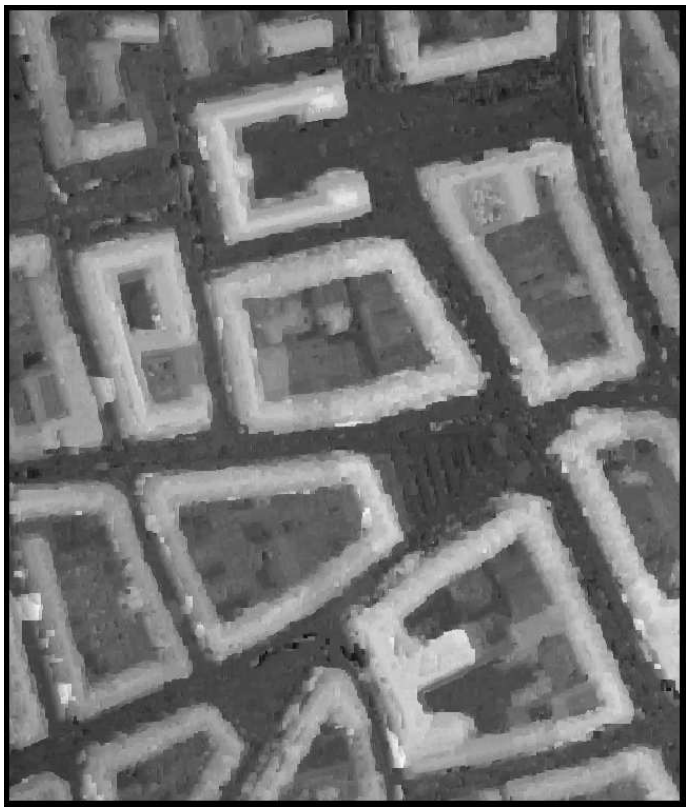

Figure 20: Digital Elevation Model of a part of Amiens, France (©IGN) obtained by satellite stereovision.

Rectangular mask	
Inside points resolution	2m
Distance of lateral bands	110m

Rectangle data term parameters	
$H_{\min}$	5m
$v_{\min}$	90%
$\sigma_{\max}$	10m

Rectangle data term weight	
ρ^r	1.2

Slices parameters	
Slices discretization step	1m
Distance between slices	1.5m
Length of slices	20m

Segment data term parameters	
$\nabla H_{\min}$	1
$\delta H_{\min}$	4m
l_{sel}	4m
δ_r	3m
η	90%

Segment data term weight	
ρ^s	3

Table 4: Data term parameters employed for processing the Digital Elevation Model presented in Figure 20.

Figure 21: Segment extraction result obtained using both processes.

5.3.1 Results

Figures 21 and 22 present the extraction result obtained using both processes. This result shows that our approach is interesting as it provides a kind of land register usefull for further analysis. In particular, our approach provides a starting point for precise building reconstruction.

Figure 22: Rectangle extraction result obtained using both processes.

Rectangular mask	
Inside points resolution	1m
Distance of lateral bands	110m

Rectangle data term parameters	
$H_{\min}$	3m
$v_{\min}$	90%
$\sigma_{\max}$	10m

Rectangle data term weight	
ρ^r	1.2

Slices parameters	
Slices discretization step	0.8m
Distance between slices	0.7m
Length of slices	20m

Segment data term parameters	
$\nabla H_{\min}$	1
$\delta H_{\min}$	2m
l_{sel}	4m
δ_r	1.5m
η	90%

Segment data term weight	
ρ^s	3

Table 5: Data term parameters employed for processing the Digital Elevation Model presented in Figure 23.

5.4 Aerial DEM

5.4.1 Presentation and parameters

We present in Figure 23 a DEM of a part of Rennes, France. It is a DEM obtained by stereovision on aerial images. This DEM is very noisy with respect to other data available (see [17]). The data term parameters employed are detailed in Table 5.

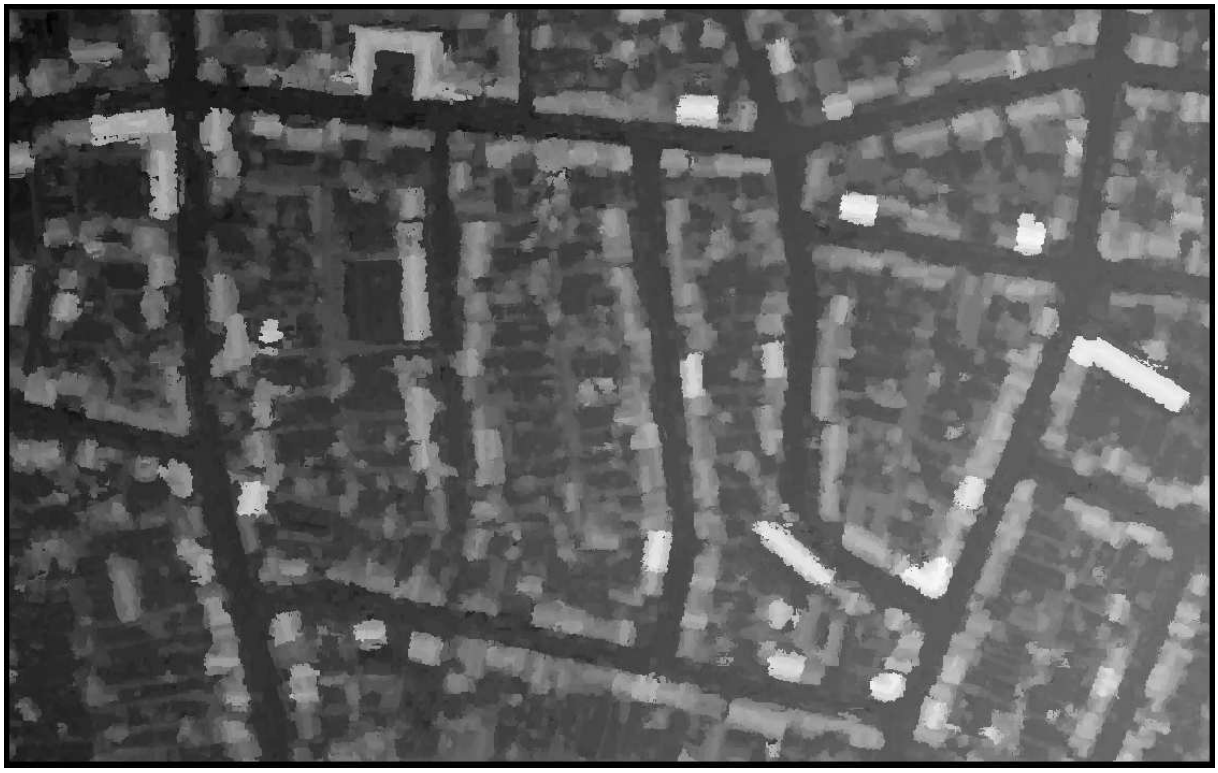

Figure 23: Digital Elevation Model of a part of Rennes, France (©IGN). This DEM has been constructed by aerial stereovision.

5.4.2 Results

Figures 24 and 25 presents the extraction result obtained using both processes.

5.5 Laser DEM

5.5.1 Presentation and parameters

We present in Figure 26 a Digital Elevation Model obtained by a Laser measurement. This piece of data originally consists in a set of sparse 3D points. The obtained DEM is consequently very smooth. On Table 6 we show the data term parameters employed.

5.5.2 Results

Figures 27 and 28 present the extraction result obtained using both processes. The results are relevant, but somehow disappointing. It seems that our approach is better for low quality DEMs than for precise data.

5.6 Comments

The algorithm requires a large number of iterations (on average 25.000.000) and a high time. Each simulation takes around 6 hours on an image of size 1000 by 1000, including approximatively 150 buildings[2]. Improving the speed of the algorithm is therefore a major issue, although the computational time depends more on the complexity of the urban area than on the size of the image. An interesting idea would be to pre-compute the result of the discontinuity filter, since it appears that

[2]Using a 3 Ghz Pentium 4 machine

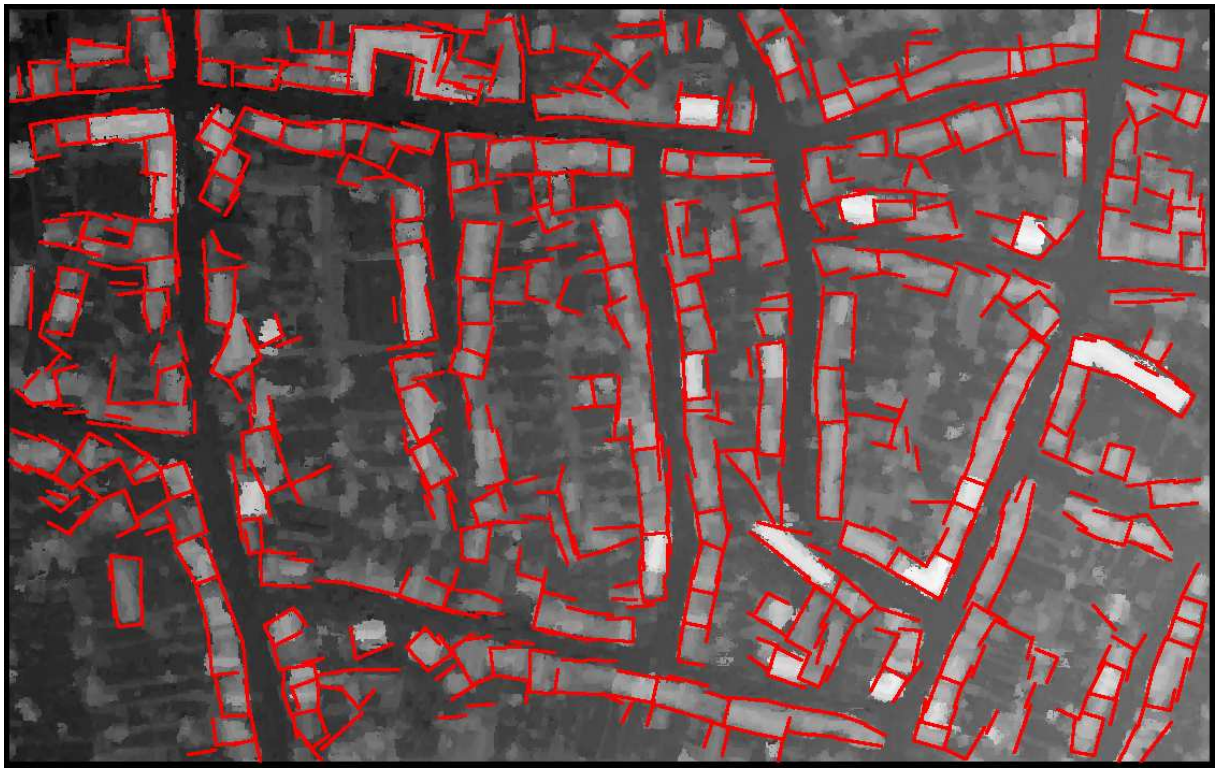

Figure 24: Segment extraction result obtained using both processes.

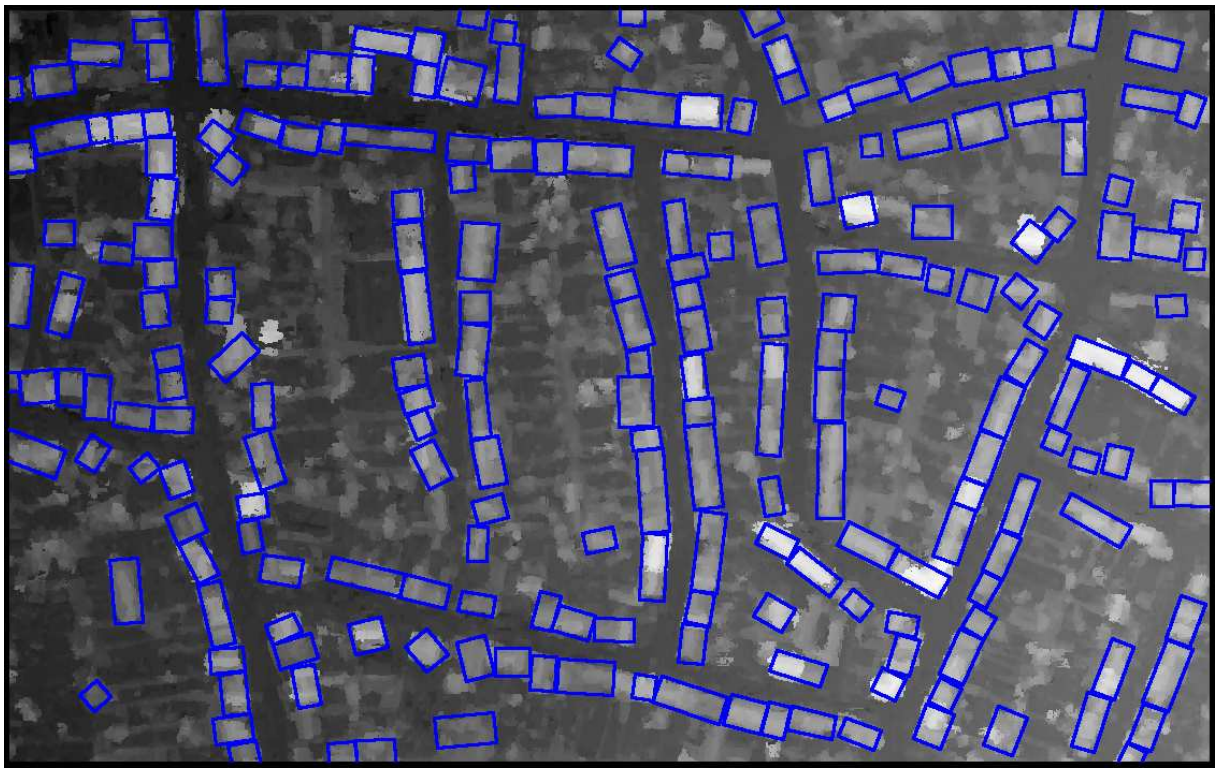

Figure 25: Rectangle extraction result obtained using both processes.

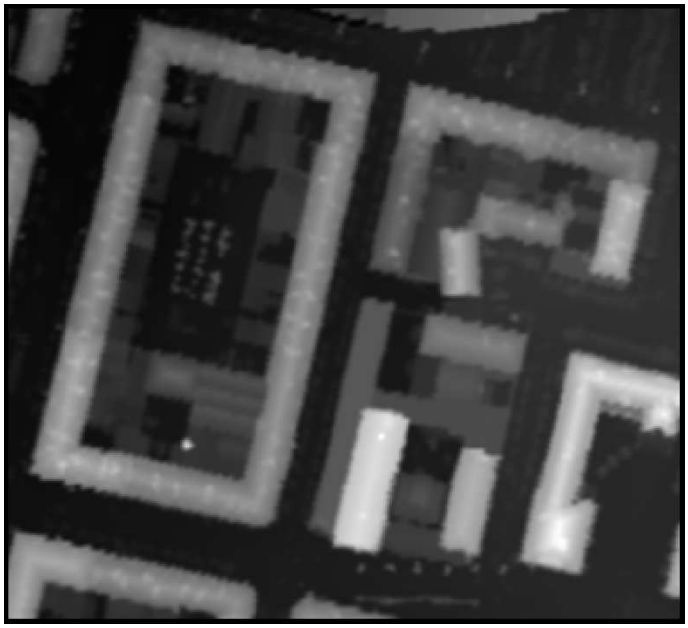

Figure 26: Digital Elevation Model of a part of Amiens, France (©IGN). This DEM has been obtained by Laser measurements, and exhibits smooth discontinuities.

Rectangular mask	
Inside points resolution	1m
Distance of lateral bands	110m

Rectangle data term parameters	
$H_{\min}$	3m
$v_{\min}$	90%
$\sigma_{\max}$	10m

Rectangle data term weight	
ρ^r	1.2

Slices parameters	
Slices discretization step	0.8m
Distance between slices	0.7m
Length of slices	20m

Segment data term parameters	
$\nabla H_{\min}$	1
$\delta H_{\min}$	2m
l_{sel}	4m
δ_r	1.5m
η	90%

Segment data term weight	
ρ^s	3

Table 6: Data term parameters employed for processing the Laser Digital Elevation Model presented in Figure 26.

Figure 27: Segment extraction result obtained using both processes.

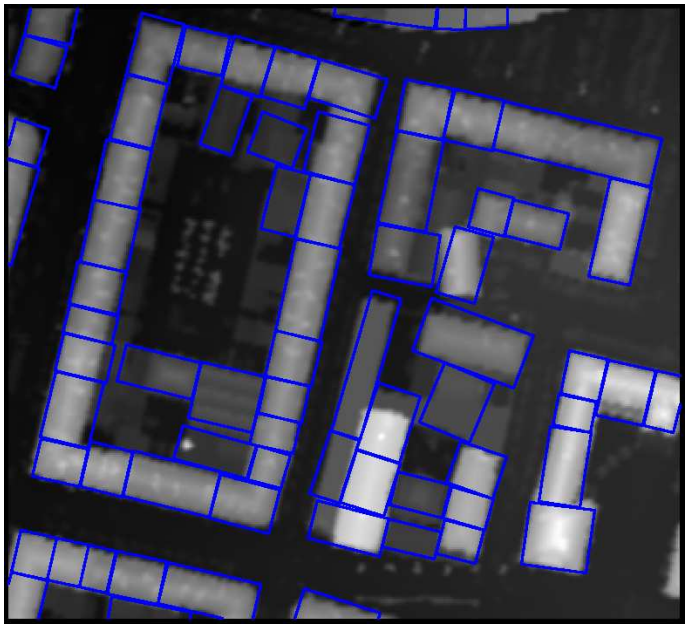

Figure 28: Rectangle extraction result obtained using both processes.

the computations associated with the segment process take most of the time. Another idea could be to keep the best objects found so far in memory.

6 Conclusion and future work

We have proposed an original approach based on stochastic geometry amenable to the introduction of a prior knowledge on both the shape of primitives to be extracted and their spatial patterns in term of their interactions.

More specifically, we have presented a model based on two types of geometrical objects. We have proposed a point process model of segments to detect discontinuities and a model of rectangles for segmenting homogeneous areas. The prior term we employ favors the connections between segments, a paving behavior of rectangles and makes both types of objects interact.

Although our approach is based on very simple objects, it proves to be powerfull when applied on real data. We have indeed been able to process Digital Elevation Models of various type (from aerial/satellite stereovision and Laser measurement). To our knowledge, few automatic methods are able to process such a variety of data.

Future work should involve the introduction of more primitives (e.g. corners, roof edges, etc...). However two major issues need to be solved in order to fully exploit this kind of model. First, the learning of parameters should be carefully examined, even if the prior model parameters proved to be very robust in practice. Second, the algorithm employed is very slow. There is a huge need for proposing new algorithms to speed up the computations. A first direction is to improve the simulated annealing. Adaptive cooling schedules are a possibility we will examine in a near future. Another interesting idea would be to test wether a memory could improve the algorithmic performances.

Acknowledgments

The authors would like to thank the the French National Geographic Institute (IGN) for providing the images presented in this report. The first author thanks the French Defense Agency (DGA) and CNRS for partial financial support during his PhD thesis.

References

[1] A. Baddeley and M. N. M. Van Lieshout. Stochastic geometry models in high-level vision. *Statistics and Images*, 1:233–258, 1993.

[2] J. Besag. On the statistical analysis of dirty pictures. *Journal of Royal Statistic Society*, B(68):259–302, 1986.

[3] A. Fischer, T. H. Kolbe, F. Lang, A. B. Cremers, W. Förstner, L. Plümer, and V. Steinhage. Extracting buildings from aerial images using hierarchical aggregation in 2D and 3D. *Computer Vision and Image Understanding*, 72(2):185–203, 1998.

[4] M. Fradkin, M. Roux, and H. Maître. Building detection from multiple views. In *ISPRS Conference on Automatic Extraction of GIS Objects form Digital Imagery*, 1999.

[5] M. Fradkin, M. Roux, H. Maître, and U. Leloglu. Surface reconstruction from multiple aerial images in dense urban areas. In *Proc of IEEE Int. Conf. on Computer Vision and Pattern Recognition*, volume 1, pages 262–267, Fort Collins, Colorado, USA, June 1999.

[6] S. Geman and D. Geman. Stochastic Relaxation, Gibbs Distributions and the Bayesian Restoration of Images. *IEEE Trans. on PAMI*, 6(6):721–741, Nov. 1984.

[7] C. J. Geyer. Likehood inference for spatial point processes. In O.E. Banorff-Nielsen, W.S Kendall, and M.N.M. Van Lieshout, editors, *Stochastic Geometry Likehood and computation*. Chapman and Hall, 1999.

[8] P.J. Green. Reversible jump Markov chain Monte-Carlo computation and Bayesian model determination. *Biometrika*, 57:97–109, 1995.

[9] H. Jibrini. *Reconstruction automatique des bâtiments en modèles polyédriques 3D à partir de données cadastrales vectorisées 2D et d'un couple d'images aériennes à haute résolution*. PhD thesis, ENST, Paris, France, 2002.

[10] C. Lacoste. *Extraction de Réseaux Linéiques à partir d'Images Satellitaires et Aériennes par Processus Ponctuels Marqués*. PhD thesis, University of Nice Sophia Antipolis, december 2004.

[11] C. Lacoste, X. Descombes, and J. Zerubia. A comparative study of point processes for line network extraction in remote sensing. *INRIA Research Report 4516*, 2002.

[12] H. Mayer. Automatic object extraction from aerial imagery-a survey focusing on buildings. *Computer Vision and Image Understanding*, 74(2):138–149, 1999.

[13] M. Ortner. *Processus Ponctuels Marqués pour l'Extraction Automatique de Caricatures de Bâtiments à partir de Modèles Numériques d'Elévation*. PhD thesis, University of Nice Sophia Antipolis, december 2004.

[14] M. Ortner, X. Descombes, and J. Zerubia. Automatic 3D land register extraction from altimetric data in dense urban areas. *INRIA Research Report 4919*, August 2003.

[15] M. Ortner, X. Descombes, and J. Zerubia. Un nouveau modèle pour l'extraction de caricatures de bâtiments sur des Modèles Numériques d'Elévation. In *TAIMA*, Hammamet (Tunisia), Octobre 2003.

[16] M. Ortner, X. Descombes, and J. Zerubia. A Reversible Jump MCMC sampler for building detection in image processing. In *Monte Carlo methods and quasi-Monte Carlo methods*, Special Session "In image Processing", Juan les Pins (France), June 2004. To appear in LNS, Springer Verlag.

[17] M. Ortner, X. Descombes, and J. Zerubia. Building outline extraction from Digital Elevation Models using marked point processes. *International Journal of Computer Vision*, 2005. To appear.

[18] A. Pievatolo and P.J. Green. Boundary detection through dynamic polygons. *Journal of the Royal Statistical Society*, B(60):609–626, 1998.

[19] H. Rue and M. Hurn. Bayesian object identification. *Biometrika*, 3:649–660, 1999.

[20] H. Rue and A. R. Syverseen. Bayesian object recognition with Baddeley's delta loss. *Adv. Appl. Prob*, 30:64–84, 1998.

[21] A. Srivastava, U. Grenander, G. Jensen, and M. Miller. Jump-diffusion Markov processes on orthogonal groups for object recognition. *Journal of Statistical Planning and Inference*, 1999.

[22] R. Stoica. *Processus Ponctuels pour l'extraction des réseaux linéiques dans les images satellitaires et aériennes.* PhD thesis, University of Nice Sophia-Antipolis, fi¿½rier 2001.

[23] R. Stoica, X. Descombes, and J. Zerubia. A Gibbs point process for road extraction from remotely sensed images. *International Journal of Computer Vision*, 37(2):121–136, 2004.

[24] D. J. Strauss. A model for clustering. *Biometrika*, 62:467–475, 1975.

[25] M. N. M. Van Lieshout. Stochastic annealing for nearest-neighbour point processes with application to object recognition. *CWI Research Report, BS-R9306, ISSN 0924-0659*, 1993.

[26] M. N. M. Van Lieshout. *Markov Point Processes and their Applications*. Imperial College Press, London, 2000.

[27] O. Viveros-Cancino. *Analyse du milieu urbain par une approche de fusion de données satellitaires optiques et radar*. PhD thesis, University of Nice-Sophia Antipolis, June 2003.

[28] G. Winkler. *Image Analysis, Random Fields and Markov Chain Monte Carlo Methods: a Mathematical Introduction*. Springer-Verlag, 2003. Second Edition.

Unité de recherche INRIA Sophia Antipolis
2004, route des Lucioles - BP 93 - 06902 Sophia Antipolis Cedex (France)

Unité de recherche INRIA Futurs : Parc Club Orsay Université - ZAC des Vignes
4, rue Jacques Monod - 91893 ORSAY Cedex (France)
Unité de recherche INRIA Lorraine : LORIA, Technopôle de Nancy-Brabois - Campus scientifique
615, rue du Jardin Botanique - BP 101 - 54602 Villers-lès-Nancy Cedex (France)
Unité de recherche INRIA Rennes : IRISA, Campus universitaire de Beaulieu - 35042 Rennes Cedex (France)
Unité de recherche INRIA Rhône-Alpes : 655, avenue de l'Europe - 38334 Montbonnot Saint-Ismier (France)
Unité de recherche INRIA Rocquencourt : Domaine de Voluceau - Rocquencourt - BP 105 - 78153 Le Chesnay Cedex (France)

Éditeur
INRIA - Domaine de Voluceau - Rocquencourt, BP 105 - 78153 Le Chesnay Cedex (France)
http://www.inria.fr
ISSN 0249-6399